

2023-05-01

A Novel Neuroinvasive Infection Modality For Francisella Tularensis Elicits Neuroinflammation Resulting In Cellular Damage

Mireya Griselle Ramos-Muniz
University of Texas at El Paso

Follow this and additional works at: https://scholarworks.utep.edu/open_etd



Part of the [Allergy and Immunology Commons](#), [Immunology and Infectious Disease Commons](#), [Medical Immunology Commons](#), and the [Neuroscience and Neurobiology Commons](#)

Recommended Citation

Ramos-Muniz, Mireya Griselle, "A Novel Neuroinvasive Infection Modality For Francisella Tularensis Elicits Neuroinflammation Resulting In Cellular Damage" (2023). *Open Access Theses & Dissertations*. 3886.
https://scholarworks.utep.edu/open_etd/3886

This is brought to you for free and open access by ScholarWorks@UTEP. It has been accepted for inclusion in Open Access Theses & Dissertations by an authorized administrator of ScholarWorks@UTEP. For more information, please contact lweber@utep.edu.

A NOVEL NEUROINVASIVE INFECTION MODALITY FOR *FRANCISELLA*
TULARENSIS ELICITS NEUROINFLAMMATION RESULTING IN
CELLULAR DAMAGE

MIREYA GRISELLE RAMOS-MUNIZ

Doctoral Program in Biosciences

APPROVED:

Charles T. Spencer, Ph.D., Chair

Eddie Castaneda, Ph.D.

Charlotte Vines, Ph.D.

Arshad M. Khan, Ph.D.

Giulio Francia, Ph.D.

Stephen L. Crites, Jr., Ph.D.
Dean of the Graduate School

Copyright ©

by

Mireya Griselle Ramos-Muniz

2023

Dedication

In loving memory of Margarita Palomo Rea.

A NOVEL NEUROINVASIVE INFECTION MODALITY FOR *FRANCISELLA*
TULARENSIS ELICITS NEUROINFLAMMATION RESULTING IN
CELLULAR DAMAGE

by

MIREYA GRISELLE RAMOS-MUNIZ, B.S.

DISSERTATION

Presented to the Faculty of the Graduate School of
The University of Texas at El Paso
in Partial Fulfillment
of the Requirements
for the Degree of

DOCTOR OF PHILOSOPHY

Department of Biological Sciences
THE UNIVERSITY OF TEXAS AT EL PASO

May 2023

Acknowledgements

I would like to thank current and past students of the Spencer, Khan, Almeida and Francia labs. Astrid Cardona and Pramod Mishra from the Cardona lab at UT San Antonio. Dr. Armando Varela and Gladys Almodovar for their kind guidance, input, and patience. To my dissertation mentor, Dr. Charles T. Spencer, your support, and encouragement have made me the scientist I am today and the scientist I long to be. To my committee members Drs. Charlotte Vines, Eddie Castaneda, Arshad M. Khan, and Giulio Francia, I deeply thank you for your scientific guidance, and support.

Abstract

Francisella tularensis (*Ft.*) is a gram-negative coccobacillus bacterium that causes the zoonotic disease tularemia in humans. *Ft.* causes the most severe, often fatal, form of the disease through inhalation. However, *Ft.* is most commonly transmitted through direct contact with infected animal carcasses such as rodents and rabbits, consumption of contaminated food or water, or through arthropod bites, particularly ticks. Due to its extremely low infectious dose, high mortality rate, and potential use as a biological warfare agent, *Ft.* is classified by the CDC as a “Tier 1 select agent”. *Ft.* infection triggers an overactive inflammatory response, termed a “cytokine storm”, which produces excessive tissue damage (and even failure) of vital organs, leading to rapid death of the host before its adaptive immunity responses can be brought to bear against the infection. In the periphery, macrophages, paradoxically the target cell for *Ft.*, provide innate immune defense against foreign material, including bacteria. Microglia, the resident macrophage-like cells of the brain and spinal cord, rapidly respond to pathological changes in the central nervous system, serving a similar function as macrophages. Their rapid activation is an important factor in guarding the neural parenchyma against infectious diseases, inflammation, and neurodegeneration while maintaining and facilitating the return to tissue homeostasis. In the United States, several clinical cases of tularemia meningitis were diagnosed since 1931; however, there is no further research exploring the condition. We hypothesize that, after peripheral inoculation of *Ft.*, the bacteria infiltrate the central nervous system using a Trojan horse-type mechanism and infect microglia, leading to overproduction of pro-inflammatory cytokines in the brain which then cause damage to surrounding neurons, ultimately leading to death. The research trajectory for this project is to: 1) identify the cellular targets of *Ft.* in the CNS; 2) identify the mechanism by which *Ft.* infiltrates

the central nervous system; and 3) determine the resulting level of neuroinflammation in the brain after infection.

Table of Contents

Dedication	iii
Acknowledgements	v
Abstract	vi
Table of Contents	viii
List of Tables	x
List of Figures	xi
Chapter 1: Background and Significance	1
1.1 <i>Francisella tularensis</i>	1
1.2 Tularemia and human disease	4
1.3 <i>Francisella tularensis</i> mechanism of infection.....	9
1.4 Meningitis, Blood-Brain Barrier, Tularemia Meningitis, and Neuroinflammation.....	14
1.4.1 Meningitis: history and occurrence.....	14
1.4.2 Blood-Brain Barrier	16
1.4.3 Tularemia meningitis	20
1.4.4 Neuroinflammation	21
1.5 Significance.....	24
1.6 Specific aims and hypothesis	25
Aim 1: Determine the cellular distribution of <i>F. tularensis</i> in the brain	25
Aim 2: Identify the mechanism LVS uses to infiltrate the central nervous system.....	25
Aim 3: Analyze the inflammatory response after intradermal inoculation with LVS	26
Chapter 2: Determine the cellular distribution of <i>F. tularensis</i> in the brain.....	28
2.1 Materials and Methods.....	28
2.2 Results.....	32
2.3 Discussion	46
Chapter 3: Identify the mechanism LVS uses to infiltrate the	51
central nervous system.....	51
3.1 Materials and Methods.....	51
3.2 Results.....	56

3.3 Discussion	71
Chapter 4: Analyze the neuroinflammatory response after intradermal inoculation with LVS	75
4.1 Materials and Methods	75
4.2 Results	79
4.3 Discussion	85
Chapter 5: Overview and final conclusions	88
References	91
Vita	102

List of Tables

Table 1: Clinical manifestations and routes of transmission of <i>F. tularensis</i>	7
Table 2. Clinical case studies of patients diagnosed with Tularemia meningitis	22
Table 3. Flow Cytometry antibody panels for suppression of macrophages in CD11b-DTR mice	54

List of Figures

Figure 1: Routes of exposure to <i>F. tularensis</i>	2
Figure 2. Global distribution of endemic <i>F. tularensis</i>	6
Figure 3. Clinical manifestation of ulceroglandular tularemia.	8
Figure 4. Model of <i>F. tularensis</i> intracellular stages in murine and human phagocytes	12
Figure 5. Innate immune recognition of <i>F. tularensis</i>	13
Figure 6. An illustration of the blood-brain barrier (BBB).....	17
Figure 7. Mechanisms of microbial traversal of the blood-brain barrier	19
Figure 8. Flow Cytometry antibody panels.....	34
Figure 9. Comparison of LVS CFU in spleen, liver, lung, and brain.	35
Figure 10. Kinetics of central nervous system invasion by LVS.....	37
Figure 12. Orthogonal image of fluorescently labeled infected microglia	40
Figure 13. Immune cells present in the brain after LVS infection captured by imaging flow cytometry	42
Figure 14. Immune cells present in the brain after LVS neuroinvasion captured by flow cytometry	44
Figure 15: Immune cell subsets carrying <i>F. tularensis</i> captured by flow cytometry.	45
Figure 16. Populations of immune cells present in the brain after LVS neuroinvasion.	58
Figure 17. Immune cell subsets present in the brain after LVS neuroinvasion	59
Figure 18. Immune cell subsets present in the brain after LVS neuroinvasion	60
Figure 19. Immune cells present in the brain after LVS infection captured by imaging flow cytometry	62
Figure 20. C57BL/6 mice LVS infected.	64

Figure 21. CD11b-DTR mice without toxin administered	65
Figure 22. CD11b-DTR mice with diphtheria toxin administered	66
Figure 23. Representation of a Transwell	68
Figure 24. Electrical resistance of Bend.3 cells in Transwells using TEER.....	69
Figure 25. Migration of macrophages.....	70
Figure 26. Inflammatory cytokines of whole brain produced in the mouse brain after LVS infection.	80
Figure 27. IL-6 and IL-1 β quantitative relation between infected and uninfected samples	83
Figure 28. Sagittal image representation of mouse anatomical brain slices	84

Chapter 1: Background and Significance

1.1 *Francisella tularensis*

Francisella tularensis (*F. tularensis*) is a gram-negative facultative intracellular coccobacillus bacterium that causes the zoonotic disease tularemia in humans [5, 6]. It was first discovered in 1912 in Tulare County, California, after reports of a plague-like illness in ground squirrels. However, those reports were not published until 1925 by Edward Francis [6]. *F. tularensis* causes the most severe, often fatal, form of the disease through inhalation of as few as ten organisms. However, *F. tularensis* is most commonly transmitted through direct contact with infected animal carcasses such as rodents and rabbits, consumption of contaminated food or water, or through arthropod bites, particularly ticks (Figure 1) [7-17]. Due to its extremely low infectious dose and high mortality rate along with its potential use as a biological warfare agent, *F. tularensis* is classified by the Center for Disease Control and Prevention (CDC) as a Category A select agent [5, 18], the highest of three categories the CDC has for high-priority organisms that pose a severe risk to national security. Other agents assigned as Category A are *Bacillus anthracis* (Anthrax), *Yersinia pestis* (bubonic plague), Variola major (smallpox), and hemorrhagic fever viruses to include Ebola, and Marburg [5, 7, 19-21].

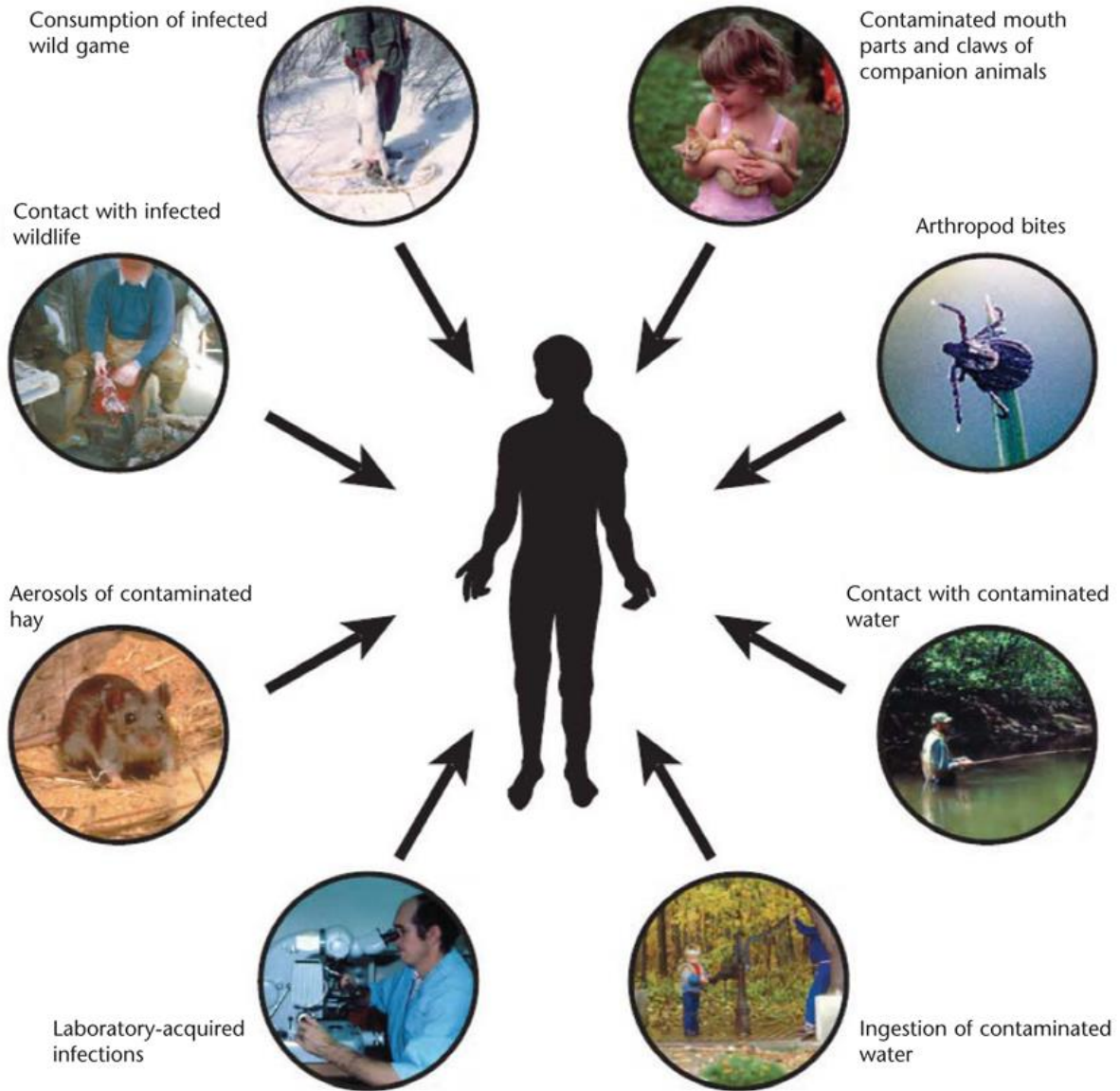


Figure 1: Routes of exposure to *F. tularensis*

F. tularensis is most commonly transmitted through direct contact with infected animal carcasses such as rodents and rabbits, consumption of contaminated food or water, or through arthropod bites, particularly ticks [7-17].

There are four strains of *F. tularensis*, each of which display different virulence profiles and geographical distributions: subspecies (subsp.) *tularensis* (Type A), *holarctica* (Type B), *novicida*, and *mediasiatica*. Of the four strains, Type A and Type B are the most important to human public health and will be the focus of this project. *F. tularensis* subsp. *tularensis* (Type A) is the most commonly isolated in North America and is the most virulent for humans. People typically become infected after touching or moving diseased or infected dead animals resulting in skin ulcers or respiratory tularemia, mowing over a dead infected animal thereby releasing aerosols, consuming or coming in contact with contaminated water, consuming meat from infected rabbits and hares (undercooked meat), and by blood-feeding arthropod vectors to include tick and biting flies [8-10, 13, 22-24]. Type A strains of *F. tularensis* have a very low infectious dose of 25 CFU when injected subcutaneously and 10 CFU when administered via inhalation of aerosol droplets. In 2016, there were 230 reported and confirmed tularemia cases in the United States, the majority of which were found in Arkansas, Oklahoma, Missouri, and Kansas [25-27].

F. tularensis subsp. *holarctica* (Type B) is found predominantly in Europe and Asia; however, there have also been reported cases in Australia [7]. Type B Francisella is less virulent than Type A and disseminates at a slower rate in humans thereby causing a milder form of tularemia. Type B Francisella has been isolated from muskrats, beavers, ground voles, and also streams, ponds, lakes, and rivers [7]. In 1942, a live attenuated vaccine was developed from Type B Francisella, called *Francisella tularensis* live vaccine strain (LVS) [28-31]. LVS has been used in human volunteer trials with some efficacy; however, LVS is not approved by the U.S. Food and Drug Administration and its use is currently restricted for military personnel and first responders. LVS is a valuable model organism as it can be manipulated in BSL-2 containment and causes a

lethal infection in mice that closely mimics the disease course of Type A-caused tularemia in humans [32].

1.2 Tularemia and human disease

Tularemia clinical cases have been reported around the world (Figure 2), predominantly during the summer and hunting seasons [32, 33]. Tularemia is particularly interesting because of its multiple routes of transmission. The risk of infection is higher in those who work in wildlife management, gardeners and landscapers, and hunters [22-24].

People who become infected after having been exposed to *F. tularensis* generally develop symptoms of disease within three to five days of exposure (Table 1) [17, 34, 35]. Although symptoms of tularemia depend largely upon the strain and route of infection, there are six major clinical manifestations known (Figure 2). Ulceroglandular tularemia is the most common form of disease (Figure 3), in which a skin ulcer will develop at the site of infection, typically from a tick bite, followed by swollen and painful lymph nodes, fever, chills, headache, and general exhaustion. Glandular tularemia evokes the same signs and symptoms as ulceroglandular tularemia, but without skin ulcers, and is typically caused by handling infected animals and carcasses, although arthropod bites have also been recorded. Oculoglandular tularemia is transmitted to the eyes after they come into contact with contaminated fingers or water. Symptoms include eye pain, swelling and discharge, an ulcer on the inside of the eyelid, and sensitivity to light. Oropharyngeal tularemia affects the mouth, throat, and digestive tract, and is typically caused by consuming contaminated meat from a wild animal or drinking contaminated water. Symptoms include fever, throat pain, mouth ulcers, vomiting, diarrhea, enlarged tonsils, and swollen neck lymph nodes. Typhoidal tularemia results from inhalation or ingestion of bacteria and causes the most severe symptoms of

disease. Patients with typhoidal tularemia will experience high fever, extreme exhaustion, splenomegaly, hepatomegaly, and in some cases pneumonia. Pneumonic tularemia typically results from inhalation of aerosolized bacteria and may go misdiagnosed as it manifests with typical signs and symptoms of traditional pneumonia to include dry cough, chest pain, and difficulty breathing. Pneumonic tularemia is the most severe form of tularemia with a mortality rate greater than 30% if left untreated [34-37]. In addition to the signs and symptoms for each of the six tularemia clinical conditions, other complications may arise, and if left untreated tularemia can be fatal. Some serious complications from tularemia disease include inflammation of the lungs causing respiratory failure, pericarditis, osteomyelitis, and bacterial meningitis resulting in severe inflammation of the meninges surrounding the brain and spinal cord.

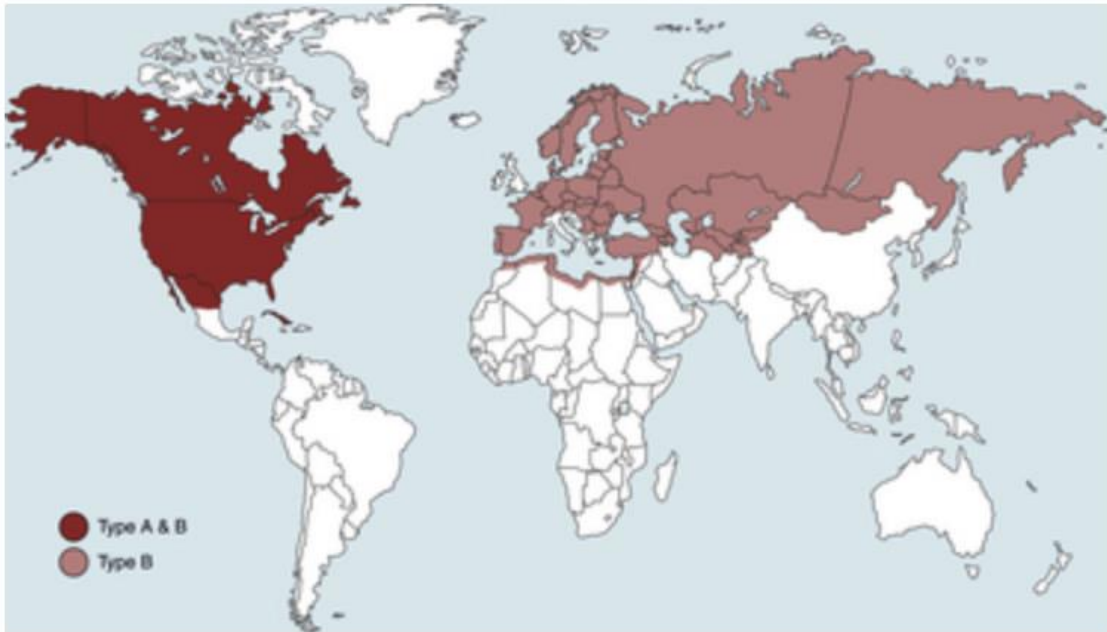


Figure 2. Global distribution of endemic *F. tularensis*

F. tularensis subsp. *tularensis* (Type A) is the most commonly isolated in North America and is the most virulent for humans. *F. tularensis* subsp. *holarctica* (Type B) is found predominantly in Europe and Asia [7, 17, 38]. Image extracted from Centers for Disease Control and Prevention.

Table 1: Clinical manifestations and routes of transmission of *F. tularensis*

Clinical manifestations, route of transmission, and clinical signs of disease after infection with *F. tularensis*. Ulceroglandular tularemia is the most common form of disease. Skin ulcers will develop at the site of infection, typically from a tick bite, followed by swollen and painful lymph nodes, fever, chills, headache, and general exhaustion. Glandular tularemia evokes the same signs and symptoms as ulceroglandular tularemia, but without skin ulcers, and is typically caused by handling infected animals and carcasses, although arthropod bites have also been recorded. [17, 38].

Clinical manifestation	Route of transmission	Clinical signs of disease
Ulceroglandular	Direct contact with rabbits and squirrels, animal bites, scratches, tick bites/mosquitoes	Skin ulcers, predominantly on hands, fever, myalgia, headache
Glandular		Absence of primary lesion
Oculoglandular	Contact with contaminated water or hands after handling infected animals	Conjunctivitis, edema of eyelids
Oropharyngeal	Ingestion of contaminated food or water	Pharyngitis, painful mucosal ulceration
Typhoidal	Not clear	Fever, vomiting, diarrhea, myalgia, chills, sepsis, meningitis
Pneumonic	Inhalation of aerosol droplets	Bronchopneumonia, Pleural effusion, Peribronchial infiltration



Figure 3. Clinical manifestation of ulceroglandular tularemia.

The image at the top left is a Google stock photo. Top right and bottom left: photos are courtesy of CDC/Dr. Brachman, 1963. Bottom right: photo was obtained from Dr. Marks [39].

1.3 *Francisella tularensis* mechanism of infection

All forms of tularemia begin by *F. tularensis* traveling from the site of infection to the regional lymph nodes where it disseminates to spleen, liver, lung, kidneys, and the central nervous system. At the macrophage surface, *F. tularensis* interacts with toll-like receptor-2 (TLR2) and stimulates production of pro-inflammatory cytokines due to the tetra-acylated lipid A structure [40, 41]. The Fc- γ receptor is the principal phagocyte receptor involved in the uptake of antibody-opsonized *F. tularensis* which then resides within the Francisella-containing phagosome (FCP) [42-45]. Newly formed FCPs acquire markers of early endosomes and late endosomes, such as EEA-1, CD63, LAMP-1, LAMP-2, and Rab7; however, the FCPs do not undergo phago-lysosome fusion. *F. tularensis* then uses a type VI secretion system to escape into the host-cell cytosol where it replicates until cell death occurs, leading to infection of neighboring cells (Figure 4) [44, 46, 47].

The initial interaction of *F. tularensis* with host cells – macrophages, dendritic cells, epithelial cells, endothelial cells, and microglia – induces the inflammatory response. Inflammation begins when host cells of the innate immune system recognize one of a multitude of pathogen associated molecular patterns (PAMPs) of an invading pathogen, e.g., bacterial DNA, LPS, and peptidoglycans [43, 44]. *F. tularensis* stimulates several signaling cascades, numbered below in relation to the numbered steps in Figure 5, to converge on initiation of the inflammatory response:

1. The surface TLR2 interaction activates NF- κ B through the MyD88 pathway, leading to the expression of pro-IL-1 β and pro-IL-18.

2. After *F. tularensis* escapes the FCP into the cytosol, it signals through the IRF-3 and TRIF pathways to produce type-I IFN [42-44, 48].
3. Signaling through the type-I interferon receptor (IFNAR) up-regulates AIM2 protein expression (consists of HIN domain and PYD domain) [42-44, 48].
4. Lysis of *F. tularensis* in the cytosol releases bacterial DNA that is recognized by the HIN domain of AIM2. The PYD domain of AIM2 then recruits the adapter protein ASC (consisting of a PYD domain and a CARD domain) which recruits procaspase-1 through its CARD domain to form the AIM2-inflammasome complex [42-44, 48].
5. Procaspase-1 proteolytically cleaves itself to generate active caspase-1. Active caspase-1 proteolytically cleaves pro-IL-1 β and pro-IL-18 to their active forms. Active IL-1 β and IL-18 initiate inflammation and trigger cell death by pyroptosis [42-44, 48].

TLR2 activation also results in the production of the pro-inflammatory cytokines RANTES, TNF- α , IL-8, IL-6, IFN- γ , and MCP-1 by peritoneal macrophages, further contributing to the inflammatory response. Other innate immune cells are additionally recruited to the area of infection and produce the effector cytokines IL-12p40, TNF- α , INF- γ , and IL-17A [42-44, 48].

During infection, cytokines have both pro-inflammatory or anti-inflammatory activities which activate or inhibit the immune response, respectively. *F. tularensis* is part of a small class of pathogens with the ability to cause disease by inducing a dysregulation in inflammatory cytokine production, termed hypercytokinemia or a cytokine storm, rather than extensive bacterial replication or toxins, as is seen in many other conditions [5, 49, 50]. This cytokine storm can be

detrimental to the host leading to severe sepsis, capillary leakage, tissue injury, and organ failure culminating in death.

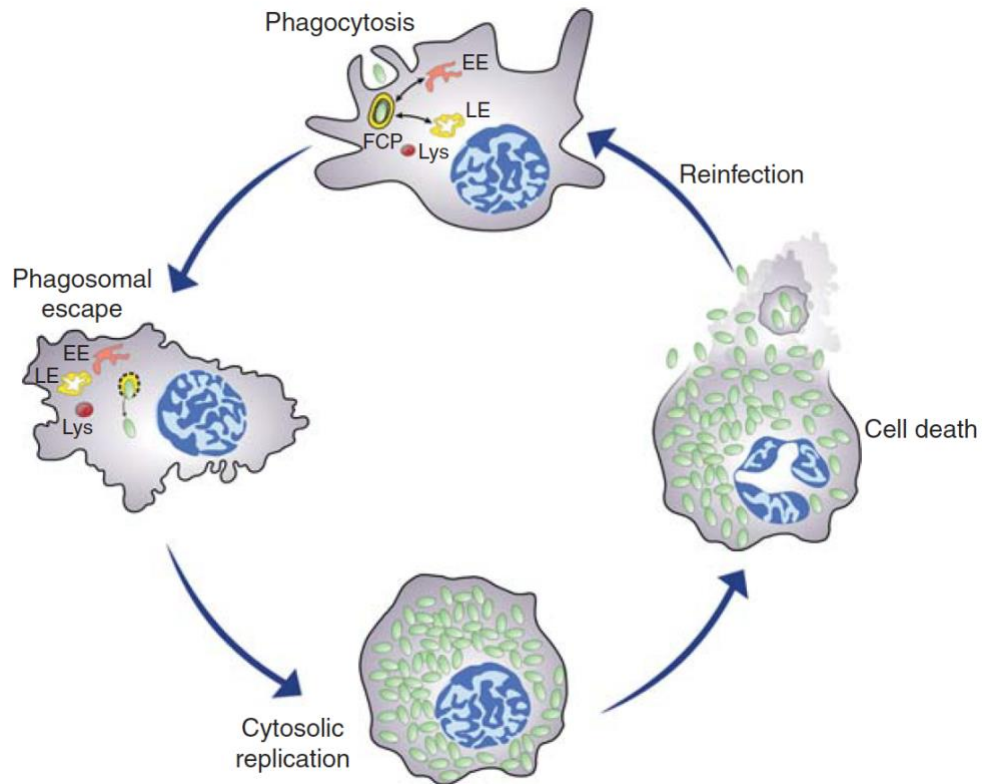


Figure 4. Model of *F. tularensis* intracellular stages in murine and human phagocytes

Tularemia begins by *F. tularensis* traveling from the site of infection to the regional lymph nodes where it will disseminate to spleen, liver, lung, kidneys, and the central nervous system. *F. tularensis* will undergo phagocytosis and *Ft.* will reside within the Francisella-containing phagosome (FCP) [42-45]. Newly formed FCPs will acquire markers of early endosomes and late endosomes, however, the FCPs will not undergo phago-lysosome fusion. *F. tularensis* then uses a type VI secretion system to escape into the host-cell cytosol where it will replicate until cell death occurs, leading to infection of neighboring cells [44, 46, 47].

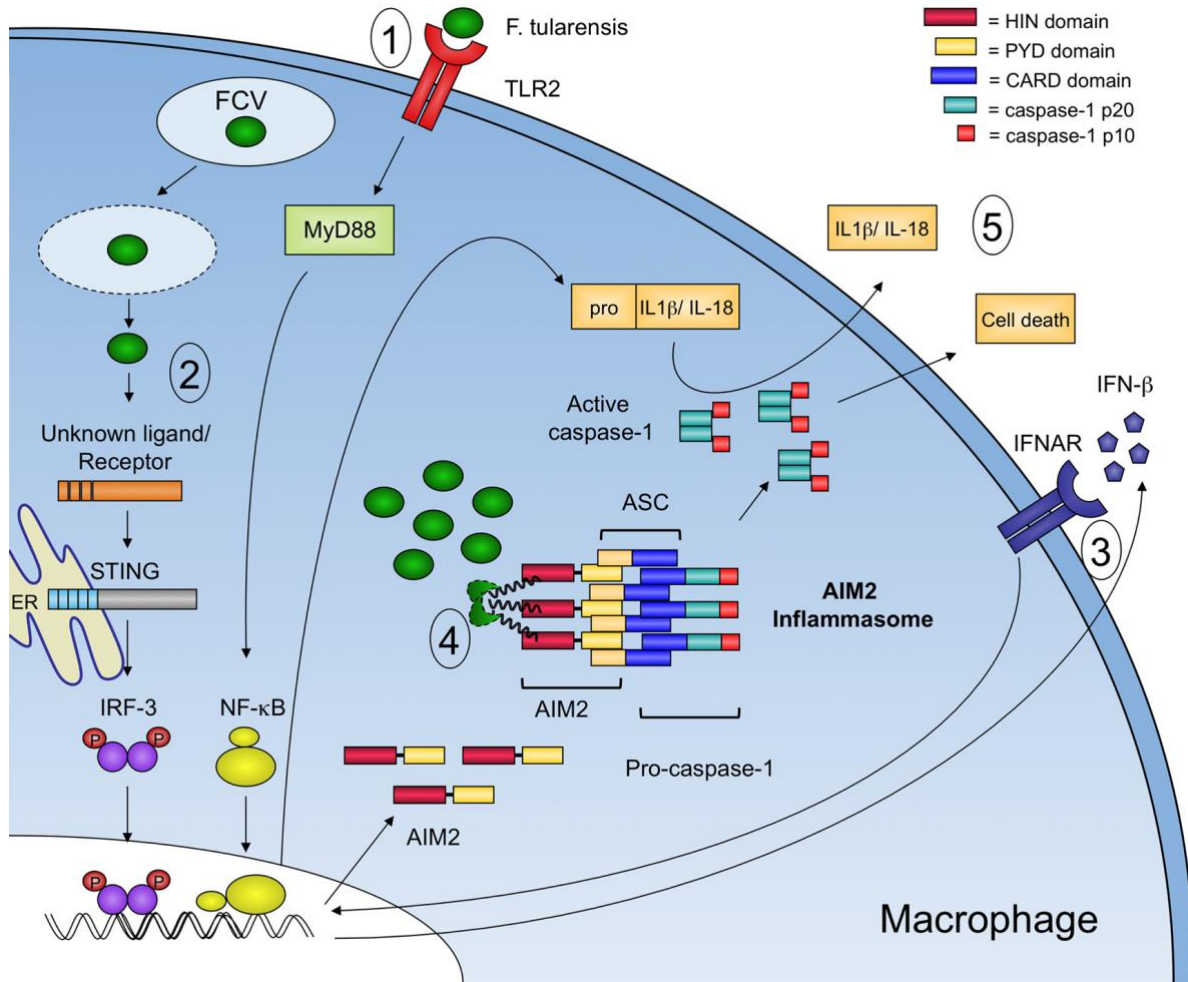


Figure 5. Innate immune recognition of *F. tularensis*

The initial interaction of *F. tularensis* with host macrophages induces the inflammatory response. Inflammation begins when host cells of the innate immune system recognize one of a multitude of pathogen associated molecular patterns (PAMPs) of an invading pathogen, e.g., bacterial DNA, LPS, and peptidoglycans. [43, 44]. *F. tularensis* stimulates several signaling cascades to converge on initiation of the inflammatory response [48].

1.4 Meningitis, Blood-Brain Barrier, Tularemia Meningitis, and Neuroinflammation

1.4.1 Meningitis: history and occurrence

Meningitis is an inflammation of the meninges that has several non-infectious and infectious etiologies. The first of these to be identified was meningococcal meningitis by Gaspard Vieusseux during an outbreak in Geneva, Switzerland, in 1805. However, it was not until 1887 that the causative agent was identified to be *Neisseria meningitidis* by Anton Weichselbaum [51]. *N. meningitidis* causes inflammation of the meninges, developmental impairment in children, severe brain damage, and can be fatal in up to 50% of cases if left untreated. Despite its presence in the brain, *N. meningitidis* can be successfully treated with a cephalosporin or prevented by vaccinations or ceftriaxone as chemoprophylaxis.

Several fungi have also been shown to cause meningitis. The most common fungal meningitis is caused by *Cryptococcus neoformans* in immunocompromised people through inhalation of spores. In healthy individuals, infection with *C. neoformans* is typically cleared whereas in immunocompromised individuals the infection can spread to the CNS and is fatal if left untreated [52]. Recently, *Candida albicans* was reported to cross the BBB and activate microglia, resulting in elevated levels of pro-inflammatory cytokines in the brain. Moreover, the fungus-induced glial granulomas (FIGGs) in the brain had concentrated amyloid precursor protein and β -amyloid peptides presumably in direct contact with the fungal cells. *C. albicans* appears to cause transient cerebritis that causes short-term memory impairment, similar to that observed in Alzheimer's disease [53].

Bacterial meningitis is associated with high mortality and morbidity rates. Bacterial pathogens typically cause an elevated inflammatory response which ultimately leads to brain

damage, including cortical necrosis, damage of the inner ear, and hippocampal apoptosis. *Mycobacterium tuberculosis*, the causative agent of tuberculosis (TB), most often infects the lungs and is spread from person to person by sneezing, coughing, or spitting. [54, 55]. Most people infected with TB are latent carriers; however, immunocompromised individuals, such as people living with HIV or diabetes, have a higher risk of developing active TB disease [54, 55]. Although rare, TB in the CNS is the most serious type of systemic TB because of its high mortality rate and serious neurological complications, such as cerebral infarction, intracerebral hemorrhage, and leptomeningeal enhancement [54, 55]. Other bacteria that are known to cause meningitis include *Salmonella* sp., *Streptococcus pneumoniae*, *Listeria monocytogenes*, *Escherichia coli*, and group B *Streptococcus*. Zoonotic bacterial meningitis is associated mainly with direct contact with infected animals or consumption of contaminated animal products and is uncommon compared to the forms discussed above [56].

Some of the most notable pathogens of the *Flaviviridae* family of viruses cause viral meningitis, such as Zika virus (ZIKV) and West Nile virus (WNV). ZIKV infections occur through the bite of an *Aedes* species mosquito. The 2015-2016 ZIKV outbreak brought the public's attention to this virus because of its vertical transmission and neural developmental problems. ZIKV crosses the placenta and replicates in the brain of the fetus, causing fetal abnormalities such as microcephaly and ocular deformation. More recently, ZIKV infection has been linked to meningoencephalitis and Guillain-Barre Syndrome [57]. The natural transmission of WNV to humans occurs through mosquito bites. The primary target cells of the virus are keratinocytes and Langerhans cells (LC) [58-60]. After infection of keratinocytes, an innate cytokine response mediated by TLR-7 is induced. This stimulates LC migration to the regional draining lymph nodes

where the virus replicates before disseminating to visceral organs and the CNS [58-60]. WNV infection causes encephalitis, meningitis, and meningoencephalitis [58-60].

1.4.2 Blood-Brain Barrier

The blood-brain barrier (BBB) is a multicellular structure at the interface of capillary vessels and the central nervous system (CNS). The luminal membrane is composed entirely of microvascular endothelial cells, while the abluminal membrane is composed of pericytes and projections from astrocytes and neurons (Figure 6) [1]. The endothelium lining of these capillaries is a crucial part of the integrity of the barrier as it regulates the intercellular tight junctions. This results in an extremely high electrical resistance of the endothelium tight junctions measuring $>1000 \text{ ohm/cm}^2$. Tight junctions within the BBB maintain homeostasis of the microenvironment in the CNS that is critical for normal neuronal function by regulating diffusion of molecules. In addition, they strictly block entry of blood-borne microorganisms, such as bacteria, viruses, fungus, and parasites.

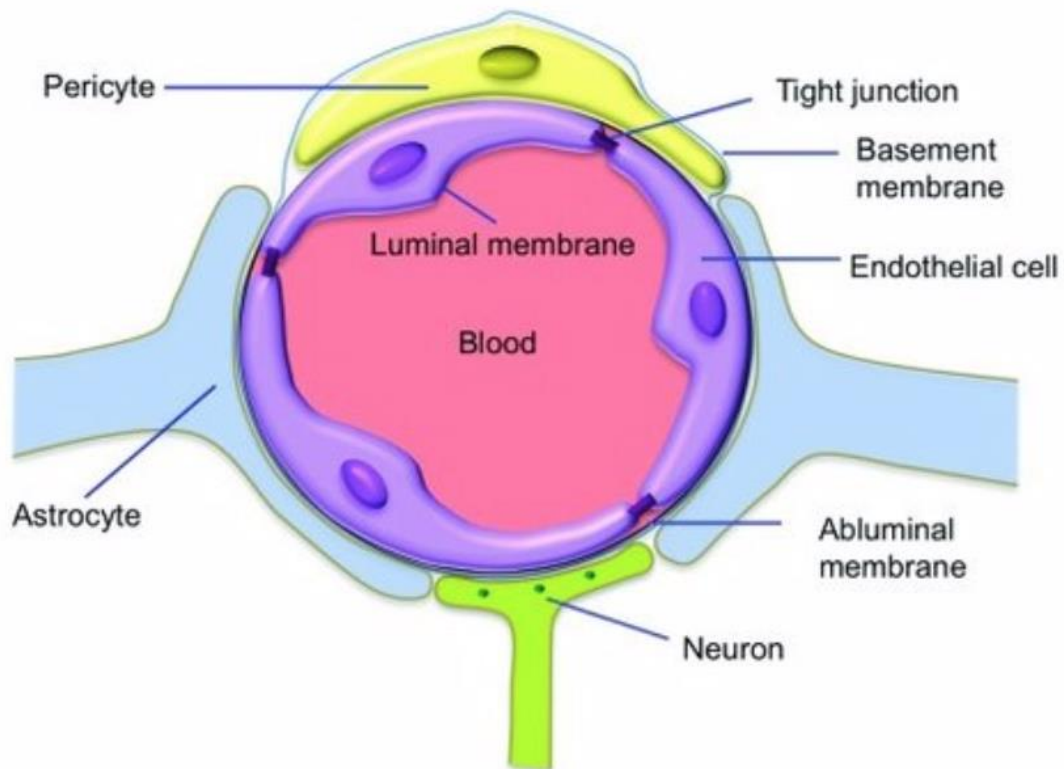


Figure 6. An illustration of the blood-brain barrier (BBB)

The luminal membrane of the blood-brain barrier (BBB) is composed entirely of microvascular endothelial cells, while the abluminal membrane is composed of pericytes and projections from astrocytes and neurons. The endothelium lining of these capillaries is a crucial part of the integrity of the BBB as it regulates the intercellular tight junctions [1].

There are few microorganisms with the ability to invade the CNS, successfully infect the brain, and cause meningitis. To breach the BBB, an extracellular pathogen must cross a monolayer of endothelial cells expressing tight junctions. Those capable pathogens have evolved different ways to penetrate the BBB. The mechanisms recognized for microbial translocation are transcellular, paracellular, and transmigration, or “Trojan horse” (Figure 7) [2-4]. In the transcellular pathway (a), microbes penetrate through human brain microvascular endothelial cells (HBMECs) without disrupting the tight junctions. Paracellular traversal (b) requires microbial penetration between barrier cells by loosening of the tight junctions with or without disrupting them. In the Trojan horse mechanism (c), pathogens penetrate the barrier while inside a phagocyte; this mechanism is commonly used by HIV-1 and West Nile virus [2-4]. Extensive research and post-mortem examinations of *N. meningitidis* infections have shown numerous bacteria interacting with the endothelium of the choroid plexuses and meninges. This suggests that there is a direct interaction between the bacteria and components of the BBB [61]. *N. meningitidis* has been localized within endothelial cells of the brain of an infected patient and was also observed to cross a monolayer of tight-junction-forming cells *in vitro*; therefore, suggesting the use of the transcellular pathway [61, 62].

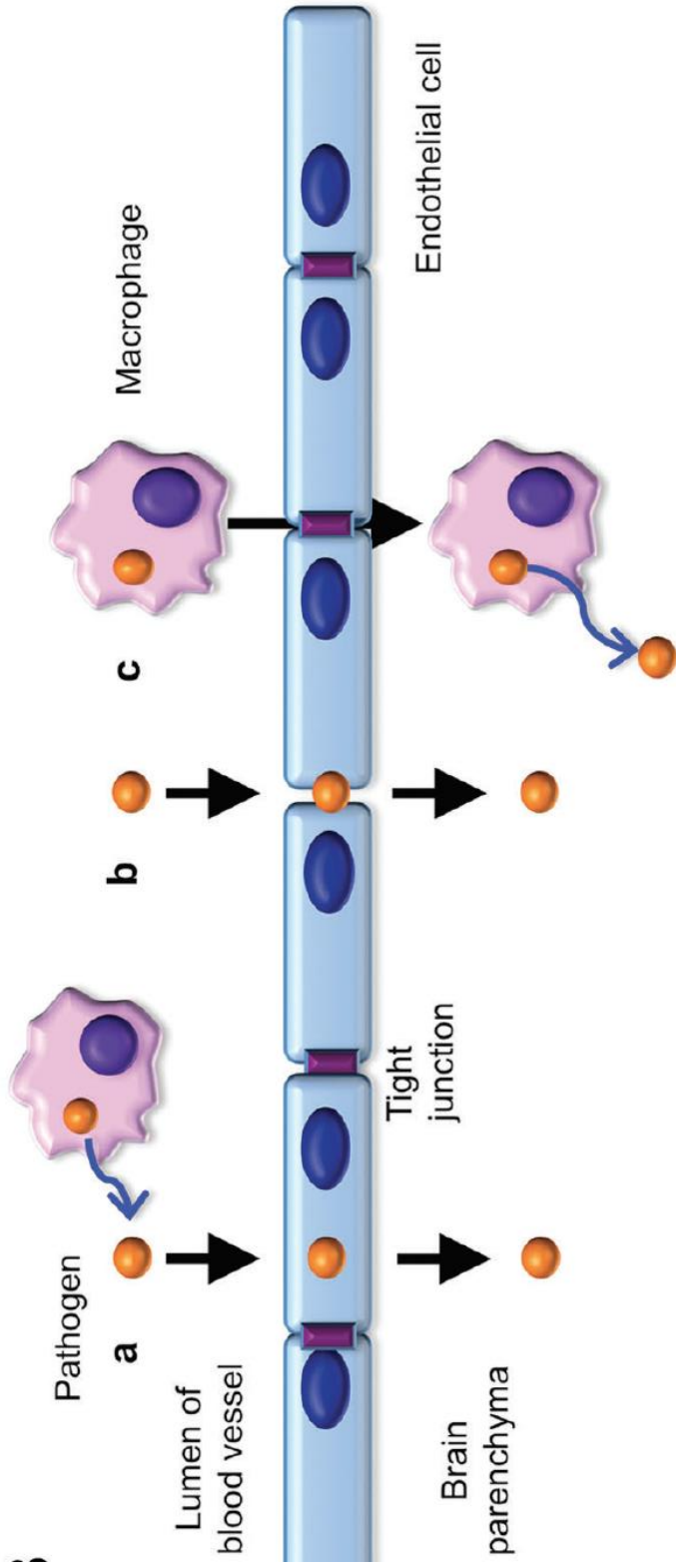


Figure 7. Mechanisms of microbial traversal of the blood-brain barrier

Extracellular pathogens must cross a monolayer of endothelial cells expressing tight junctions. The mechanisms recognized for microbial translocation are transcellular, paracellular, and transmigration, or 'Trojan horse'. In the transcellular pathway (a), microbes penetrate through human brain microvascular endothelial cells (HBMECs) without disrupting the tight junctions. Paracellular traversal (b) requires microbial penetration between barrier cells by loosening of the tight junctions with or without disrupting them. In the Trojan horse mechanism (c), pathogens penetrate the barrier while inside a phagocyte [1-4]

1.4.3 Tularemia meningitis

In case studies of tularemia meningitis, there have been 20 diagnosed clinical cases of tularemia meningitis since 1931; however, there is no research exploring the extent of the disease[63]. In these clinical case reviews, *F. tularensis* was detected by serology of patient's cerebrospinal fluid (CSF), and isolation of blood bacteria (Table 2) [63]. The patient demographics are diverse: five female patients ranging from 4-years old to 51-years old, and 12 male patients ranging from 5-years old to 64-years old. These findings are compatible with other reports that suggest males are at a higher risk for infection than females [64-67]. In the 1930's, blood transfusion from a survivor of tularemia was a common treatment for tularemia meningitis. From 1931 to 1945, all cases resulted in patient death, which occurred within 5–11 days after initial onset of meningitis symptoms. Primary tularemia infection presented as ulceroglandular lesions in seven patients, oropharyngeal infection in four patients, and typhoidal tularemia in six patients. In 1949, a 16-year-old female who presented a primary infection of ulceroglandular tularemia also showed symptoms of tularemia meningitis and was later confirmed by blood and CSF cultures. The patient was then treated with anti-tularemia horse serum administered intrathecally 155 days after first symptoms of disease and was the first recorded patient to recover from tularemia meningitis. From 1985 to 1996, the preferred treatment for tularemia meningitis was chloramphenicol alone or combined with one or more of the following: rifampicin, gentamicin, streptomycin, or tetracycline. Since 1998, the preferred treatment for tularemia meningitis has been a combination of two of the following: gentamicin, doxycycline, ceftriaxone, streptomycin, or chloramphenicol, however, it is of the utmost importance that treatment begins immediately following exposure [63]. The last reported death from tularemia meningitis was a 17-year old male with a primary infection of an ulceroglandular lesion after a tick bite in 2004 [63]. The patient

was diagnosed by blood and CSF serology. He was treated with ceftriaxone at an unknown number of days from first symptoms of meningitis.

1.4.4 Neuroinflammation

Systemic inflammation generates inflammatory messengers that are sent to the brain and ultimately lead to activation of microglia, not unlike activated macrophages in the periphery. After an injury, the peripheral nervous system has the capacity for regeneration, whereas the CNS capacity is very limited. Recently identified lymphatic vessels in the meninges indicate a link between the CNS and the peripheral immune system [68]. Mast cells have a potential to communicate from the periphery to the CNS since they are located close to peripheral nerves and within the brain and meninges, where they can mediate the inflammatory response [69]. The interaction between mast and glia cells contributes greatly to neuroinflammation, particularly if the system is stressed, as is the case during a systemic infection of tularemia. When the BBB is disrupted, the infiltration of pro-inflammatory cytokines recruits other cells and molecules to the CNS and the overwhelming amount of inflammation that is induced by these events often results in neuronal injury [70].

Table 2. Clinical case studies of patients diagnosed with Tularemia meningitis

Clinical case studies of tularemia meningitis in the United States detailing patient demographics, source of infection, primary infection, method of diagnosis of meningitis, and outcome [63].

Source	Patient sex/age	Work	Source of infection	Days from first symptom to meningitis	Primary infection	Diagnosis	Treatment	Outcome
Haizlip and O'Neil, 1931	M/45 y	Night watchman	Rabbit or squirrel	5	Ulceroglandular	Bacterial isolation from blood	None	Death
Bryant and Hirsch, 1931	M/48 y	Chef	Rabbit	8	Ulceroglandular	Bacterial isolation from blood	None	Death
Hartman, 1932	M	Butcher	Rabbit	9	Ulceroglandular	Serology	Blood transfusion from survivor of tularemia	Death
Pund and Hatcher, 1937	F/12 y	None	Unkown	8	Oropharangeal	Serology	None	Death
David and Owens, 1944	F/5 y	None	Cat	11	Ulceroglandular	Bacterial isolation from blood and CSF	None	Death
Stuart and Pullen, 1945	M/34 y	Unkown	Unkown	5	Typhoidal	Bacterial isolation from blood	None	Death
Fields, 1949	F/16 y	Unkown	Rabbit	155	Ulceroglandular	Bacterial isolation from blood	Antitularemia horse serum intrathecally and intravenously, chloramphenicol, streptomycin	Recovered with sequelae
Hutton and Everett, 1985	M/60 y	Unkown	Tick	9	Typhoidal	Serology	Chloramphenicol, streptomycin	Recovered
Lovell et al, 1986	M/13 mo	None	Cat	59	Oropharangeal	Bacterial isolation from blood, and CSF serology	Chloramphenicol	Recovered
Harper et al, 1986	M/18 mo	None	Unkown	8	Oropharangeal	Bacterial isolation of CSF and serology	Chloramphenicol	Recovered
Hill et al, 1990	M/64 y	Unkown	Unkown	7	Typhoidal	Bacterial isolation of CSF and serology	Chloramphenicol, rifampicin, gentamicin	Recovered
Alfes and Ayers, 1990	M/19 y	Construction	Rabbit	7	Oropharangeal	Bacterial isolation from CSF	Streptomycin, chloramphenicol	Recovered
Pittman, 1996	M/5 y	None	Rabbit	3	Typhoidal	Bacterial isolation from CSF	Chloramphenicol, streptomycin, tetracycline	Recovered
Rodgers et al, 1998	F/4 y	None	Unkown	9	Ulceroglandular	Bacterial isolation from CSF	Gentamicin, doxycycline	Recovered
Weiner et al, 2004	M/17 mo	None	Tick	Unknown	Ulceroglandular	CSF serology and bacterial isolation from CSF	Ceftriaxone	Death
Gangat, 2007	F/51 y	Unkown	Rabbit	30	Typhoidal	Bacterial isolation from CSF	Streptomycin, doxycycline	Recovered with sequelae
Hofinger et al, 2009	M/21 y	Landscaper	Rabbit	7	Typhoidal	Bacterial isolation from CSF	Streptomycin, chloramphenicol, ceftriaxone, vancomycin,	Recovered
Contentin et al, 2011	M/68 y	Unkown	Tick	7	Unknown	CSF serology and bacterial isolation from CSF	acyclovir, thiamphenicol, gentamycin	Recovered
Ducatez et al, 2022	M/64 y	Unkown	Hare carcasses	8	Ulceroglandular	Serology, ELISA	amoxicillin, ceftriaxone, acyclovir, ciprofloxacin	Recovered
Nemmour et al, 2019	M/5 y	None	Mouse	8	Oropharangeal	Serology	amoxicillin-clavulanate, gentamicin, doxycycline	Recovered

IL-6 has been shown to have a role in neurogenesis, during which it influences both neurons and glia, both in a healthy CNS and during neuronal injuries and conditions that induce neuroinflammation [71-74]. There is also research suggesting that some astrocyte and other glial cell lines express IL-6 when stimulated with IL-1 β [71-74]. IL-1 β along with TNF- α have been shown to induce IL-6 in cultured neurons and astrocytes [71-74]. High levels of IL-1 β expression recruit leukocytes to the CNS. They also induce activation of astrocytes, microglia, and the expression of pro-inflammatory cytokines [75].

In a 2017 *in vitro* study, primary cultured cerebellar granule neurons incubated with IFN- γ quickly induced neuronal apoptosis [76]; however, in a co-culture with astrocytes, the neurons seemed to be protected from the effects of IFN- γ . The same investigative group conducted an *in vivo* study where they challenged C57BL/6 mice with LPS with and without IFN- γ stimulation. The inflammation induced by LPS followed by anti-IFN- γ resulted in neuron apoptosis, further supporting their results from the *in vitro* experiment. However, they found that astrocyte-secreted IL-6 resulted in neuroprotection by IFN- γ . This led to the conclusion that inflammatory stimulation quickly activated astrocytes and provided protection against neuronal damage [76].

TNF- α is a pro-inflammatory cytokine that is involved in the innate immune response as well as in the CNS where it has homeostatic and pathophysiological functions [77-79]. In the normal CNS, TNF- α has a regulatory function that is essential for learning, plasticity, memory, and sleep [80-84]. However, when the CNS is under stress, astrocytes and microglia secrete large amounts of TNF- α and further increase neuroinflammation [77, 85].

1.5 Significance

In the United States, there have been 20 diagnosed clinical cases of tularemia meningitis since 1931; however, there is no research exploring the extent of the disease. In these clinical case reviews, patient demographics are diverse: five female patients ranging from 4-years old to 51-years old and 12 male patients ranging from 5-years old to 64-years old. In other reports, it is suggested males are at higher risk for infection than females [64-67]. From 1931 to 1945, all cases resulted in patient death, which occurred within 5–11 days after initial onset of meningitis symptoms. Research of *F. tularensis* in the CNS is vital to further knowledge of tularemia disease and the inflammation that is caused in the brain after infection. Furthermore, continued study of the CNS using LVS as a model would help in the understanding of neuronal damage and the breakdown of the blood-brain barrier following the neuroinflammation that is caused by *F. tularensis* infection. In this study we will show cell targets of LVS, targeted and general inflammation that occurs after infection in brain tissue, and the infection mechanism used to traverse the blood-brain barrier by *F. tularensis*.

1.6 Specific aims and hypothesis

Aim 1: Determine the cellular distribution of *F. tularensis* in the brain

Bacteria were identified in the mouse brain after peripheral inoculation of male mice with LVS. In order to determine the kinetics of central nervous system invasion by LVS, brains from LVS-inoculated mice were serially harvested every 8 hours starting at 24 hours post-infection and ending 96 hours post-infection. Brains were homogenized and plated on modified Mueller-Hinton agar plates. In order to determine whether the bacteria are productively infecting neural cell types, brain coronal-plane tissue sections were stained with anti-IBA-1 or anti-GFAP to target microglia and astrocytes, respectively. These sections were imaged by confocal microscopy to visualize the cell populations and brain regions being infected by LVS. Flow cytometric analyses complimented confocal imaging to quantify the proportions of infected cell types.

Aim 2: Identify the mechanism LVS uses to infiltrate the central nervous system

Immune cell subsets carrying *F. tularensis* after peripheral inoculation were identified by inoculating mice with APC-labeled LVS, isolating leukocytes using a Percoll density gradient followed by flow cytometry. Isolated leukocytes were stained with antibodies to target peripheral and neural immune cells, including macrophages, microglia, and astrocytes, and subsequently analyzed using flow cytometry. APC⁺ cell populations were interrogated further by gating for microglia, macrophages, and astrocytes as defined by the antibodies used. Immune cell subsets targeted by *F. tularensis* after peripheral inoculation were visualized by imaging flow cytometry

in collaboration with the University of Texas at San Antonio to observe bacterial load. To elucidate the role of peripheral macrophages in bacterial CNS invasion, CD11b-DTR transgenic mice were treated with diphtheria toxin to deplete macrophages prior to infection with LVS. To determine whether *F. tularensis*-infected macrophages can transit the blood-brain barrier, mouse-derived endothelial cells were used to construct an *in vitro* model of the blood-brain barrier. Endothelial translocation of LVS-infected macrophages was tested through a Transwell migration assay with the use of an 8 μm pore membrane.

Aim 3: Analyze the inflammatory response after intradermal inoculation with LVS

The overall neuroinflammatory response in the mouse brain after peripheral intradermal inoculation with LVS was analyzed in total brain homogenate using a MilliPlex multiplex assay with the following panel of markers: IL-1 β , IL-2, IL-6, IFN- γ , IL-12p70, TNF- α , IL-22, IL-23, IL-17A, IL-27, GM-CSF, IL-18, IL-10, IL-4, IL-5, IL-9, and IL-13. To determine if the neuroinflammatory response varies within the brain, an Adult Mouse Brain Slicer matrix was used to cut eight rostral to caudal slices (~1.5 thick). Gene expression of the inflammatory cytokines IL-1 β and IL-6 was quantified by qRT-PCR.

We hypothesize that, following peripheral intradermal inoculation with *F. tularensis* (LVS), the bacteria cross the blood-brain barrier and infiltrate the central nervous system using a Trojan horse-type mechanism. This allows for infection of microglia and leads to an overproduction of pro-inflammatory cytokines in the brain, in a manner similar to that observed in the periphery, which may cause damage to surrounding neurons, ultimately leading to disease and potentially death.

Chapter 2: Determine the cellular distribution of *F. tularensis* in the brain

2.1 Materials and Methods

Animal procedures

All animal procedures were carried out in accordance with the Guide for the Care and Use of Laboratory Animals [86] and approved by the Institutional Animal Care and Use Committee of the University of Texas at El Paso. Male C57BL/6 mice between six to eight weeks old were used in all studies. They were maintained on a 12-hour light/dark cycle with *ad libitum* access to food and water. For intradermal injection, bacterial stocks were diluted to the appropriate concentration in sterile PBS. Mice were anesthetized with 3-5% isoflurane and injected intradermally in the flank above the hindquarters with 1×10^6 pre-labeled LVS bacteria suspension using sterile PBS in a volume of 50 μ l. Animals were monitored every 12 hours for the first 48 hours, then every 8 hours thereafter. All animals were weighed before inoculation and every morning thereafter and were monitored for clinical symptoms of disease. An animal was considered terminal when it had lost 20% of its baseline weight or if became lethargic and immobile with prodding. All animals were humanely euthanized per the American Veterinary Medical Association standards and organ harvest was performed 72 hours post-infection, unless otherwise noted. Once an animal was euthanized, its chest cavity was exposed, and a blunt needle was inserted into the heart through the left ventricle towards the aorta and clamped into place. Sterile PBS was then used to perfuse the animal until its vasculature was apparently cleared of blood; this was followed by perfusion with chilled *p*-formaldehyde buffered in sodium borate (pH 9.5). The brain was removed from the skull

and placed in fixative solution overnight at 4°C. The brain was then frozen with supercooled hexane and stored at –80°C.

F. tularensis holarctica (LVS) was obtained from Denise Monack (Stanford University) and was grown on chocolate agar plates at 37°C for 24 – 48 hours. Plates were scraped aseptically, and the bacteria harvested into sterile PBS to be washed. Bacteria were labeled using a concentration of 100 µM of *BacLight* bacterial stain and washed to remove excess dye. Bacteria was then resuspended into sterile PBS with 20% glycerol and stored at –80°C.

Comparison of LVS Colony Forming Units in various organs

LVS was inoculated intradermally in the flank above the hind quarters of C57BL/6 mice with 1×10^6 cells in 50 µL of sterile PBS. Spleen, liver, lung, and brain were harvested 72 hours post-infection, homogenized and plated on modified Mueller Hinton plates, and were incubated for 48 hours at 37°C. Subsequently CFUs were calculated.

Kinetics of central nervous system invasion by LVS

LVS was inoculated intradermally in the flank above the hind quarters of C57BL/6 mice with 1×10^6 cells diluted in 50 µL of sterile PBS. Mice were perfused as described above, and brains harvested serially every 8 hours starting at 24 hours post-infection and ending 96 hours post-infection. Brains were homogenized and plated on modified Mueller-Hinton agar plates. Bacterial load was subsequently calculated at each time point.

Visualization of LVS in the mouse brain

Coronal-plane frozen sections were made using a Leica CM3050S cryostat at a 30 μm thickness. All sections were placed into cryoprotectant and stored at 4°C. Brains were divided into six 1-in-6 series. Using PBS, sections were rinsed of cryoprotectant (five rinses, five minutes each, '5 \times 5') and were then incubated in 2% normal donkey serum (EMD-Millipore) blocking solution and 0.1% Triton X (Sigma-Aldrich) for 2–3 hours at room temperature. Sections were incubated in a solution of rabbit anti-IBA-1 (Wako) to target microglia for 16–18 hours at 4°C, and then rinsed with PBS (5 \times 5). Sections were then reacted with biotinylated donkey anti-rabbit IgG (Jackson), or biotinylated donkey anti-goat IgG (Jackson) secondary antibody cocktail for 5-6 hours at room temperature, and then rinsed with PBS 5 \times 5. Secondary antibodies were then made fluorescent by being conjugated with Alexa Fluor 488 (Jackson) and tissues counterstained with Neurotrace 435/455 (Thermo Fisher Scientific), or DAPI (4',6-diamidino-2-phenylindole) (Thermo Fisher Scientific) for 1 hour at room temperature using photo-protective conditions, then rinsed once more with PBS 5 \times 5. Sections were mounted on positively charged Superfrost slides (Thermo Fisher Scientific), air-dried, and coverslipped with sodium bicarbonate-buffered glycerol, sealed with clear nail polish, and stored at 4°C for further analysis. The same staining protocol was repeated using goat anti-GFAP (Santa Cruz) to target astrocytes. Alternatively, after sectioning, tissue was directly mounted onto positively charged Superfrost slides for staining using the SNAP ID system (EMD Millipore Bioscience) followed by the same staining procedures listed above. All antibodies and fluorophores were diluted in blocking solution. Tissue sections were then

imaged using a Zeiss LSM 700 confocal system located within the Cytology, Screening and Imaging Core Facility of the University of Texas at El Paso. The lasers used were: 405 nm, 488 nm, 555 nm, and 693 nm. All tissue sections were surveyed using x20, x40 oil, and x63 oil objectives.

Identification of immune cell subsets carrying *F. tularensis* after peripheral inoculation by flow cytometry

For the identification of immune cell subsets carrying *F. tularensis* after peripheral inoculation, perfused brains were placed in 3 ml of sterile HBSS without Ca^{+2} , and Mg^{+2} (Gibco) in a 5ml round bottom tube and were homogenized using a sterile Dounce homogenizer (10A/10B). Final volume was adjusted to 7 ml with HBSS. 3 ml ISP was added to make the brain homogenate 30% Percoll (GE Healthcare). In a 15 ml tube containing 70% Percoll, the brain homogenate-30% Percoll was slowly overlaid using a transfer pipette. This was centrifuged at 500xg for 30 minutes at room temperature without the brake on the centrifuge. After centrifuge, most of the top layer was removed by vacuum until 1 ml was left from the interface, the interface was then transferred on top of a 50 ml conical tube with a cell strainer. The cell strainer was washed by adding 10ml HBSS on top of the strainer, then centrifuged at 1,300 rpm for 10 minutes at 4°C. The pellet was resuspended with 1ml of staining buffer, then the cells counted. Cells were centrifuged at 1,300 rpm for 10 minutes at 4°C then resuspend in 100µl of FACS buffer in a 96-well round bottom plate. Fc shield (anti-CD-16/CD-32) was then added and incubated for 15 minutes at room temperature. 50µl of antibody master-mix (Figure 8a) was added and incubated for 30 minutes, then centrifuged for 2 minutes at 2,000 rpm. Cells were washed with 100µl of

FACS buffer and centrifuged for 2 minutes at 2,000 rpm. Buffer was removed 100µl pre-warmed CytoFix/CytoPerm was added and incubated for 15 minutes. 200µl of 1x PermWash was added then plate centrifuged for 2 minutes at 2,000 rpm. Buffer was removed and cells resuspended with 100µl of master-mix cocktail of internal antibodies (Figure 8a), incubated for 20 minutes. 200µl of 1x PermWash was added and centrifuged the cells for 2 minutes at 2,000 rpm. Cell pellets were resuspended in 200µl FACS buffer and transfer to 5ml round bottom tubes to analyze through flow cytometry using the Beckman Coulter Gallios at the Cytometry, Screening and Imaging Core Facility at the University of Texas at El Paso. Alternatively, antibody panel in Figure 8b was used and cell pellets were resuspended in 50µl FACS buffer then transfer to 1.5ml Eppendorf tubes, wrapped in parafilm and shipped overnight on cold packs to UT San Antonio to analyze using the Amnis ImageStream X imaging flow cytometer in the Biophotonics Core Facility.

2.2 Results

To determine the bacteria load in known peripheral organs targeted by LVS (spleen, liver, lung) in comparison to the brain, LVS was inoculated intradermally in the flank above the hind quarters of C57BL/6 mice with 1×10^6 cells diluted in 50 µL of sterile PBS. In order to ensure that any bacteria detected was present in the parenchymal tissue, the animals were perfused with 5 volumes saline following sacrifice to rinse out blood from the organs. Spleen, liver, lung, and brain were harvested 72 hours post-infection, homogenized and plated on modified Mueller Hinton plates, and were incubated for 48 hours at 37°C. As expected from previous studies, the spleen had the highest bacteria load at 1.1×10^9 CFU, followed by liver with 4.8×10^8 CFU, then lung with 7.3×10^7 CFU. Although significantly lower than these organs, the brain did show an appreciable

bacterial load with 4.3×10^3 CFU (Figure 9). Thus, despite the lower level of brain CFUs, LVS was consistently found in each mouse.

a.

Antibody	Fluorophore
Iba-1	FITC
GFAP	PE
CD45	PE-CF594
CD140a	PE-Cy5
CD23	PE-Cy7
BacLight	APC
Ly6G	APC-Cy7
CD11b	PacBlue
SiglecF	BV510

b.

Antibody	Fluorophore
Iba-1	FITC
GFAP	PE
CD45	PE-CF594
CD140a	PE-Cy5
CD11b	PacBlue
SiglecF	BV510
Ly6C	BV605
BacLight	APC
Ly6G	APC-Cy7

Figure 8. Flow Cytometry antibody panels

Antibody panels used for flow cytometry and imaging flow cytometry. a) Flow Cytometry antibody panel for cytometry performed at The University of Texas of El Paso using the Beckman Coulter Gallios at the Cytometry, Screening and Imaging Core Facility. b) Imaging flow cytometry antibody panel for cytometry performed in collaboration with UT San Antonio using the Amnis ImageStream X imaging flow cytometer in the Biophotonics Core Facility.

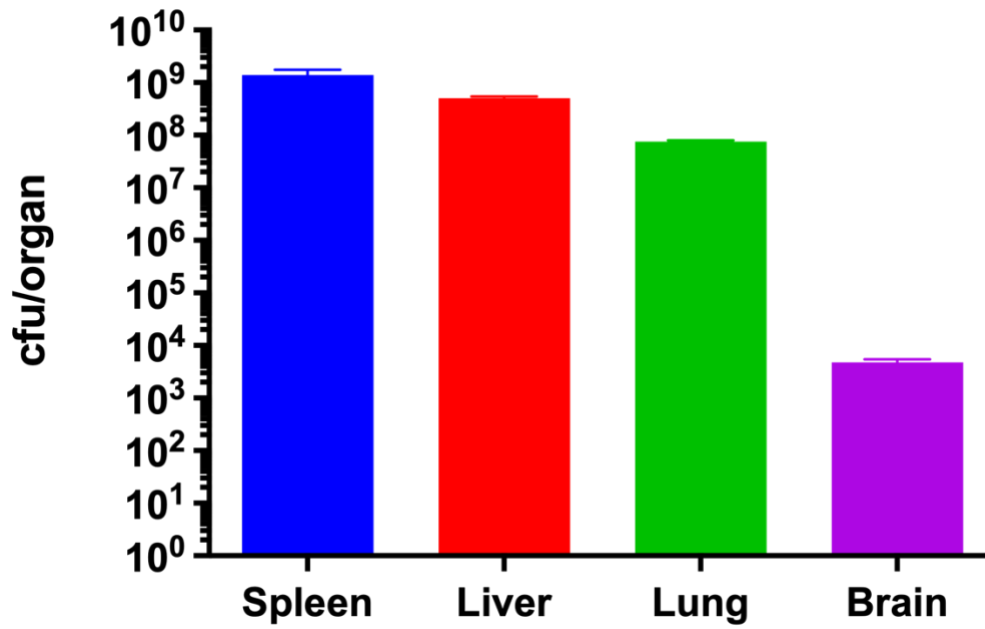


Figure 9. Comparison of LVS CFU in spleen, liver, lung, and brain.

LVS was inoculated intradermally in the flank above the hind quarters of C57BL/6 mice with 1×10^6 cells in 50 μL of sterile PBS. Spleen, liver, lung, and brain were harvested 72 hours post-infection, homogenized, plated on modified Mueller Hinton plates, and were incubated for 48 hours at 37°C.

To determine the kinetics of accumulation of LVS in the CNS, brains were harvested every 8 hours starting at 24 hours post-infection and ending 84 hours post-infection from mice intradermally infected with LVS on the flank above the hind quarters. As above, the total brain homogenate was plated on modified Mueller-Hinton agar plates for CFU determination. Our time course study revealed that LVS traverses the BBB as soon as 42 hours post infection with an average of 40 bacteria cells (Figure 10). Bacteria load then peaks at an average of 1.75×10^5 CFU around 60 hours post infection. A drop in bacteria load is then observed, and around 84 hours post infection until time of death a low-plateau in bacteria load that averages about 100 bacteria cells is detected. This accumulation could be explained by either continued entrance of the bacteria into the brain or replication of bacteria within the brain.

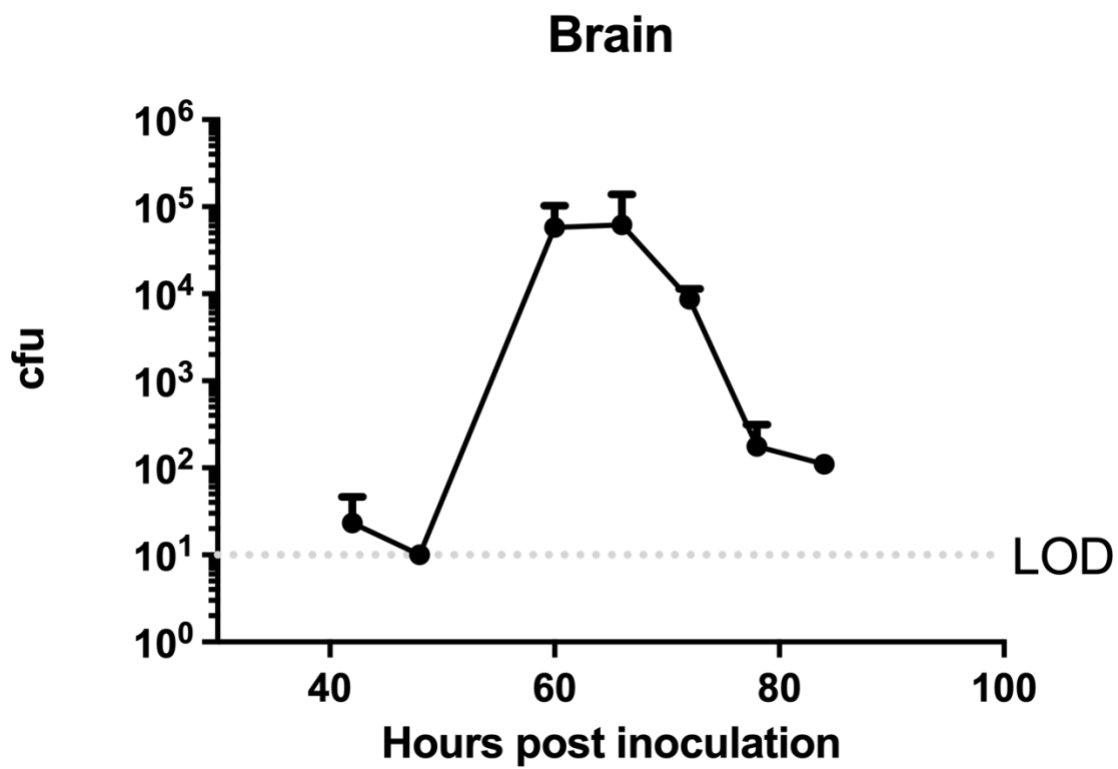


Figure 10. Kinetics of central nervous system invasion by LVS

Male mice were inoculated with LVS, perfused, and brains harvested serially every 8 hours starting at 24 hours post-infection and ending 84 hours post-infection. Brains were homogenized and plated on modified Mueller-Hinton agar plates.

Knowing that bacteria is accumulating in the brain tissue itself, we next sought to visualize the bacteria in the brain as well as determine its cellular association by using confocal microscopy of coronal-plane frozen sections. These sections were stained with Neurotrace to identify neuronal cell bodies (blue) and antibodies to identify microglia cells (anti-Iba1, green) or astrocytes (anti-GFAP, green) and LVS pre-labeled with *BacLight* Red (red). No red staining was observed in uninfected tissue demonstrating specificity of the *BacLight* Red signal (Figure 11). We observed that both microglia and astrocytes were infected by *BacLight* Red-labeled LVS. It was observed that an average of 1-2 LVS bacterial cells infect one microglia cell, while an average of 2-3 LVS bacterial cells infect one astrocyte cell on average.

Despite the thin sections in Figure 11, it is possible that in these images the bacteria are situated in a different plane of section within the tissue either above or below the cell being imaged. In order to demonstrate that the bacteria are inside of the cell, we performed a z-stack image series and can see through the orthogonal projection that the red fluorescent signal is indeed contained inside of the green fluorescent signal labeling the targeted cell (Figure 12).

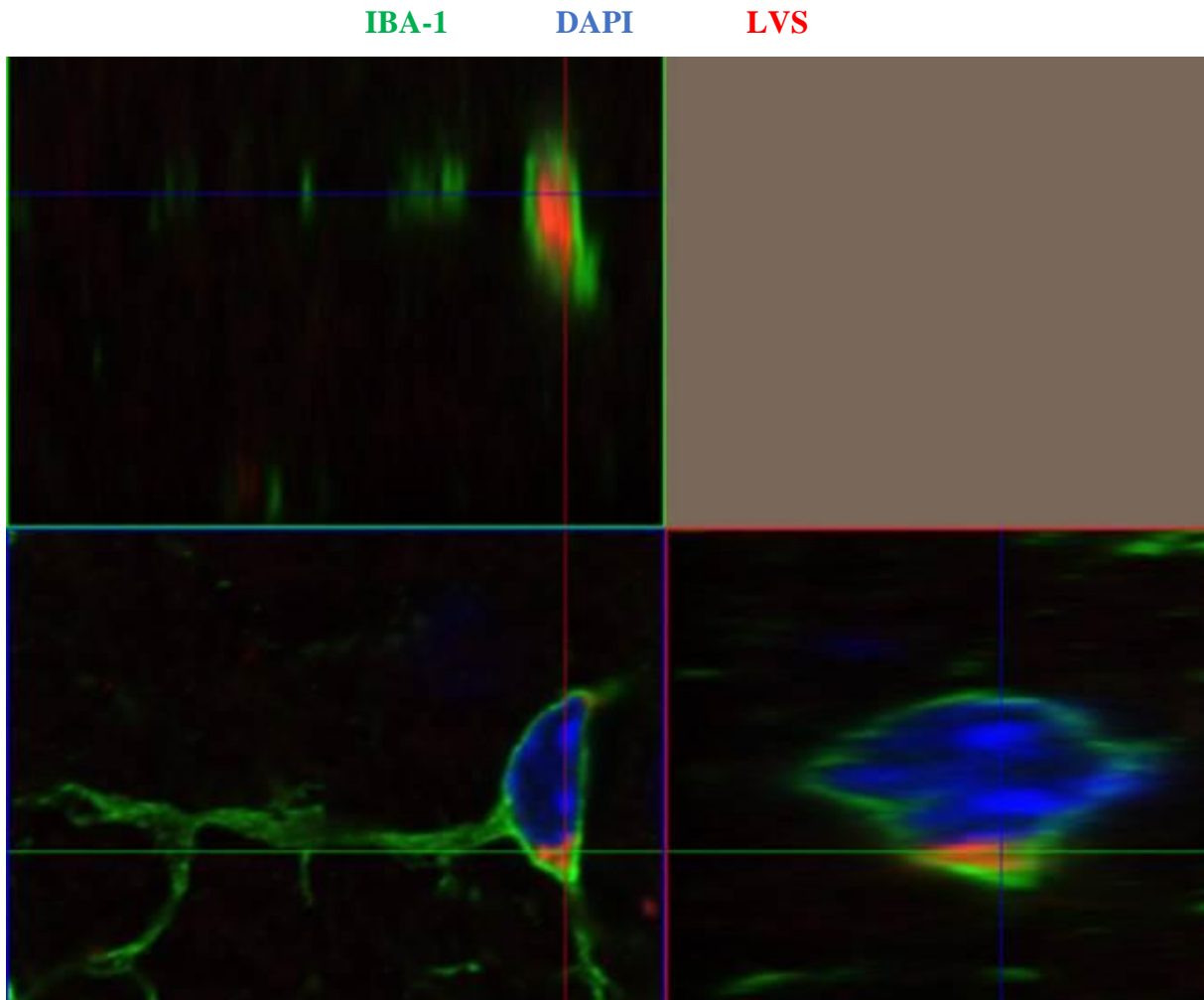


Figure 12. Orthogonal image of fluorescently labeled infected microglia

Infected microglia in the brain. LVS labeled with *BacLight Red* (red) was injected intradermally. Brain was fixed, harvested, sectioned, and counterstained with DAPI (4',6-diamidino-2-phenylindole) (blue). Microglia (green) were labeled using anti-Iba-1 produced in rabbit at 1:1,000.

To comprehensively visualize the level of infectivity in microglia and astrocytes, single cell brain homogenates isolated from animals infected with *BacLight Red* pre-labeled LVS were stained for microglial and astrocytic cell markers and analyzed with the Amnis ImageStream X imaging flow cytometer by the Biophotonics Core at the University of Texas at San Antonio (Figure 13). Based on the bacterial fluorescent signaling (red), bacteria were detected in both microglia and astrocytes. The intensity of the fluorescent signal appeared high in astrocytes compared with microglia consistent with confocal observations of more bacteria present in astrocytes.



Figure 13. Immune cells present in the brain after LVS infection captured by imaging flow cytometry

Immune cell subsets carrying *F. tularensis* after peripheral inoculation were identified with the use of imaging flow cytometry. Leukocytes were isolated by Percoll density gradient from perfused animals and was followed by profiling of immune cell subsets in collaboration with UT San Antonio by use of the Amnis ImageStream X imaging flow cytometer.

To further elucidate the immune cell subsets carrying *F. tularensis* after peripheral inoculation, single cell brain homogenates were analyzed by flow cytometry. Perfused brains were harvested and homogenized, leukocytes isolated by Percoll density gradient, and stained with a cocktail of antibodies (Figure 8a) to identify cell types. The cells were then resuspended in FACS buffer and analyzed through flow cytometry using the Beckman Coulter Gallios Flow Cytometer in the Cytometry, Screening and Imaging Cell Core at the University of Texas at El Paso. Gating of the fluorescent signal from the *BacLight* Red-labeled LVS, we verified that both astrocytes and microglia were present in the infected cell population in addition to oligodendrocytes (Figure 14 and 15). Of the infected cell population, oligodendrocytes composed 26.9%, microglia composed 29.9%, and astrocytes composed 13.2% of brain cells positive for LVS (Figure 15a). When observing for the mean fluorescence intensity it was found that microglia had the highest MFI at 354, followed by astrocytes at 317, and lastly oligodendrocytes had an MFI of 306 (Figure 15b).

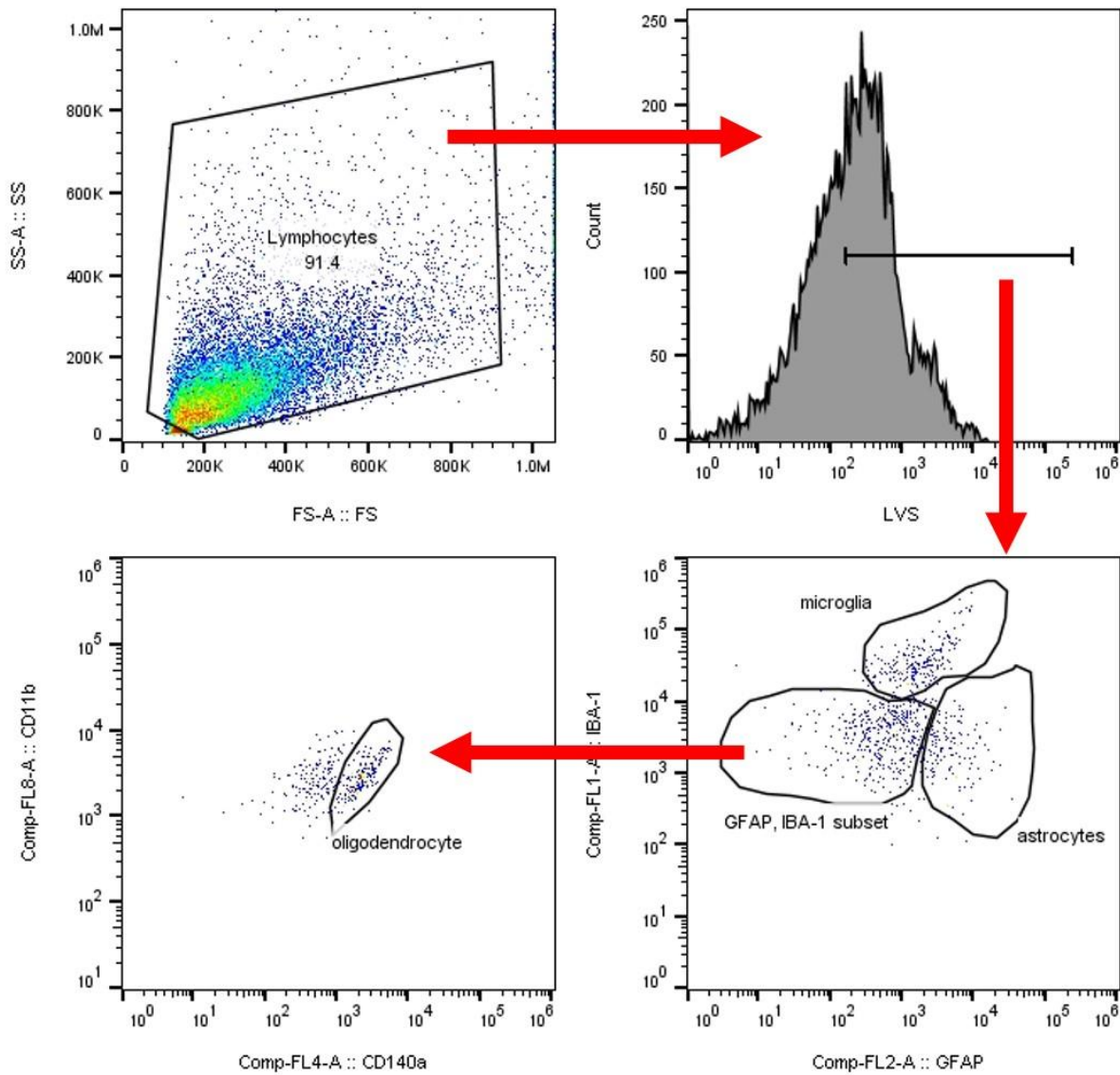


Figure 14. Immune cells present in the brain after LVS neuroinvasion captured by flow cytometry

Immune cell subsets carrying *F. tularensis* after peripheral inoculation were identified with the use of flow cytometry. Leukocytes were isolated by Percoll density gradient from perfused animals and was followed by profiling of immune cell subsets by use of the Gallios Flow Cytometer from Beckman Coulter.

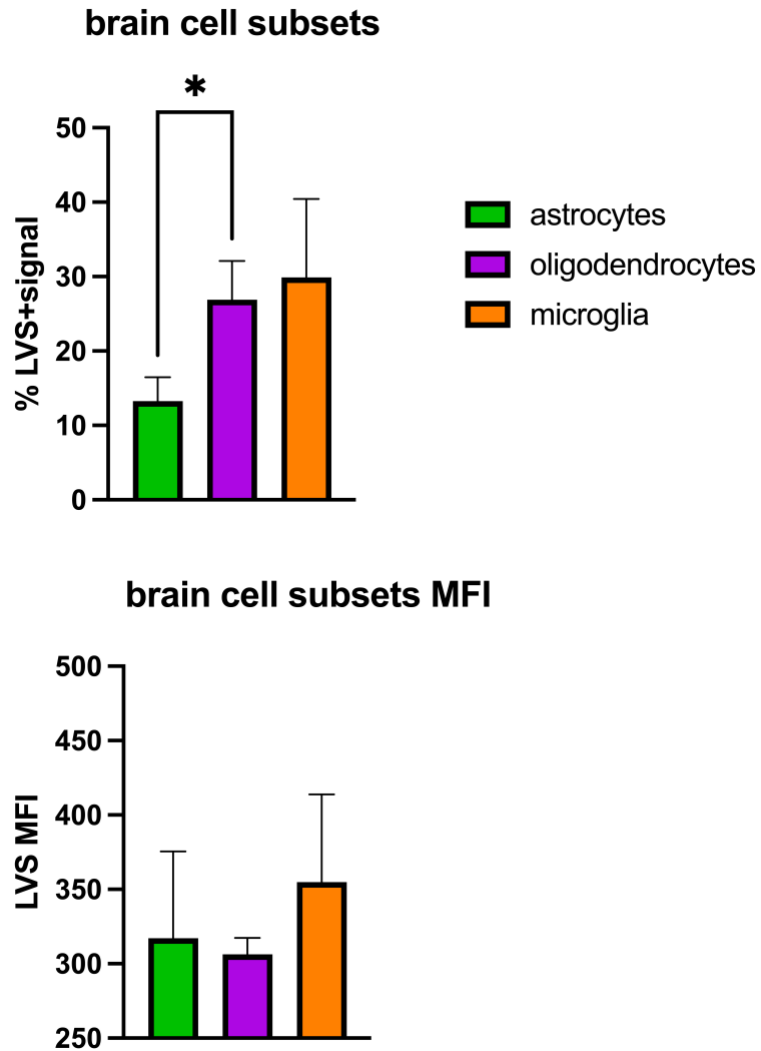


Figure 15: Immune cell subsets carrying *F. tularensis* captured by flow cytometry.

Immune cell subsets carrying *F. tularensis* after peripheral inoculation were identified with the use of flow cytometry. Leukocytes were isolated by Percoll density gradient from perfused animals and was followed by profiling of immune cell subsets by use of the Gallios Flow Cytometer from Beckman Coulter.

2.3 Discussion

This study represents the first report of active *F. tularensis* infection in the brain parenchyma. Previous clinical reports of tularemia meningitis mention disease in the CSF following a primary infection, however, these reports did not detect productive bacterial infection of neural cells. Our data showed evidence of active infection in brain tissue of mice intradermally infected with LVS that began accumulating in the brain 42 hours post-infection and peaked at 60 hours post-infection. We observed that both microglia and astrocytes were infected by invasive *F. tularensis*.

The identification in difference of LVS load between spleen, liver, lung, and brain harvested 72 hours post-infection found that spleen has the highest bacteria load at 1.1×10^9 CFU, followed by liver with 4.8×10^8 CFU, then lung with 7.3×10^7 CFU, and brain with 4.3×10^3 CFU. Though in the periphery CFUs are much higher, it was evident in each sample that LVS infection was present in brain tissue and exploring this condition further was necessary. It is possible that previous studies of *F. tularensis* have failed to research tularemia meningitis due to the several logs difference in bacterial load, however, as this study shows, even a lower bacterial burden by peripheral-organ comparison leads to a destabilization of CNS tissue homeostasis. In the case of *L. monocytogenes*, it has been reported that in BALB/c mice after intravenous injection, there is a bacterial burden detected in the brain before and after perfusion of about 10^3 CFU at 72 hours post-infection [87]. Disease progression and bacterial burden of *S. pneumoniae* is a bit peculiar, a research group reported that BALB/c mice infected through tail intravenous injection and harvested at 8 hours post-infection had a blood bacterial burden of 10^8 CFU, the authors noted that all mice in the cohort showed clear evidence of severe pneumococcal disease at this time point, and that given the signs and symptoms of disease these would eventually make progress to

meningitis [88]. The limit of detection (LOD) represents the minimum number of bacteria that can be detected by this assay, and is influenced by several factors, to include the number of bacterial cells initially present in the sample, and in this case, the LOD is 1 CFU. The limitation imposed by the LOD in CFU plating represents an important factor that needs to be considered in this assay.

Brain frozen sections of infected and uninfected mice were incubated in a solution of rabbit anti-IBA-1 to target microglia, and goat anti-GFAP to target astrocytes. It is observed that an average of 1-2 LVS bacterial cells infect one microglia cell. It is also observed that an average of 2-3 LVS bacterial cells infect one astrocyte cell on average. It is consistent in every confocal image that astrocyte cells have 2-3 LVS cells and sometimes more associated with the labeled astrocyte cell. Labeled microglia cells are typically associated with 1-2 LVS cells, seldomly we will observe a higher number of LVS cells. This observation suggests a possibility that astrocytes are shouldering a larger bacterial burden than microglia during LVS infection, and should be explored further. Our observations are the first to report microglia and astrocyte cells being actively infected by *F. tularensis holarctica* (LVS) since the first clinical reports of tularemia meningitis in 1931. Given that our study only tested for IBA-1 and GFAP antibodies, we cannot exclude the possibility of other cell types being targeted by LVS. During troubleshooting stages of this experiment, we attempted staining with oligodendrocyte progenitor cells antibody CD140a, macrophage antibody CD68, endothelial cell antibody CD105, and endothelial cell antibody CD31. Staining with these antibodies proved to be unsuccessful, in part due to some of the listed antibodies were not meant for this application, and it is my personal belief that some of the listed antibodies were not of quality as they were free samples from the manufacturer. In a final attempt to help the antibodies work, antigen retrieval was performed on multiple occasions and proved to be unsuccessful with CD68, CD31, and CD140a. Further studies are needed to identify other possible cell targets of

LVS in the CNS through confocal microscopy. Confocal microscopy has become a widely used imaging technique that allows for the visualization of cells and tissue with high resolution and specificity. One of the most significant limitations of confocal microscopy is its restricted field of view, where only a few cells can be visualized within the optical field at any given time and should be carefully considered. Instead of single-fixed field of view, one could potentially do a tile scan in a conventional confocal microscope, alternatively, the use of a light sheet microscope would also be a suitable alternative.

Having confirmed the presence of LVS in the brain, it was necessary to identify the time point at which *F. tularensis* crosses the blood-brain barrier and invades general brain tissue. Our time course study revealed that LVS traverses the BBB as soon as 42 hours post infection with an average of 40 bacteria cells. Bacteria load then peaks at an average of 1.75×10^5 CFU at 60 hours post infection. A drop in bacteria load is then observed, and 84 hours post infection until time of death a low-plateau in bacteria load that averages about 100 bacteria cells is detected. Though there are no dedicated kinetic studies available for *L. monocytogenes*, *S. pneumoniae*, or *M. tuberculosis*, the most similar pathogen thus far would be *L. monocytogenes* which reports infection of the CNS 72 hours post intravenous injection in BALB/c mice [87]. This study has provided an understanding of the exact time LVS traverses the BBB, this information is critical to calculate the appropriate duration of animal infection and timing of tissue harvest. This study only explored the first 84 hours post infection and observed a low-plateau occur at this time point. It would be interesting to investigate if continued serial collection would continue to observe a low-plateau, or alternatively if LVS is cleared from the CNS at a certain time point. It is again important to note the LOD in CFU plating represents a critical factor that needs to be considered in this assay.

To elucidate and visualize the level of infectivity in microglia and astrocytes, single cell brain homogenates from animals infected with LVS that had been pre-labeled with *BacLight Red* were stained for microglia and astrocyte cell markers and analyzed with the Amnis ImageStream X imaging flow cytometer by the Biophotonics Core at the University of Texas at San Antonio. Based on the bacterial fluorescent signaling, bacteria were detected in both microglia and astrocytes. The intensity of the fluorescent signal appeared high in astrocytes when compared with microglia which confirms our confocal imaging findings. The capability of imaging flow cytometry to analyze a limited number of cells per assay is a constraining factor that needs to be considered when using this technology.

To get a more comprehensive picture of the immune cell subsets carrying *F. tularensis* after peripheral inoculation, single cell brain homogenates were analyzed by flow cytometry. Perfused brains were harvested and homogenized, leukocytes isolated by Percoll density gradient, and stained with a cocktail of antibodies to identify cell types. The cells were then resuspended in FACS buffer and analyzed through flow cytometry using the Beckman Coulter Gallios Flow Cytometer in the Cytometry, Screening and Imaging Cell Core at the University of Texas at El Paso. Gating of the fluorescent signal from the *BacLight Red*-labeled LVS, we corroborated that both astrocytes and microglia were present in the infected cell population, in addition to an observed population of infected oligodendrocytes.

The possibility exists that our experimental design may not have encompassed all cell types relevant to this study. Other studies have demonstrated that various bacteria, including *L. monocytogenes*, *M. tuberculosis*, and *S. pneumoniae*, are capable of infecting both microglia and astrocytes [89-91]. It remains certain that the brain consistently demonstrated a lower bacterial burden when compared to spleen, liver, and lung. This could be further explained by the nature of

the blood-brain barrier and its efficacy of maintaining a much more sterile environment than periphery organs. We have ascertained that *F. tularensis* productively infects the brain parenchyma and indeed has particular cellular targets such as astrocytes, microglia, and oligodendrocytes. The query now becomes the method or mechanism by which LVS is able to traverse the BBB and infect its cell targets.

Chapter 3: Identify the mechanism LVS uses to infiltrate the central nervous system

3.1 Materials and Methods

All animal procedures were carried out in accordance with the Guide for the Care and Use of Laboratory Animals [86] and approved by the Institutional Animal Care and Use Committee of the University of Texas at El Paso. Male C57BL/6 mice between six to eight weeks old were used in all studies, they were bred and maintained as described in Chapter 2. For intradermal injection, mice were anesthetized with 3-5% isoflurane and injected intradermally in the flank above the hindquarters with 1×10^6 pre-labeled LVS bacteria suspension using sterile PBS in a volume of 50 μ l. Animals were monitored and evaluated for clinical symptoms of disease as described in Chapter 2. All animals were humanely euthanized per the American Veterinary Medical Association standards and organ harvest was performed 72 hours post-infection, unless otherwise noted. Once an animal was euthanized, its chest cavity was exposed, and a blunt needle was inserted into the heart through the left ventricle towards the aorta and clamped into place. Sterile PBS was then used to perfuse the animal until its vasculature was apparently cleared of blood. The brain was then stored as noted in the following protocols.

F. tularensis holarctica (LVS) was obtained from Denise Monack (Stanford University) and was grown on chocolate agar plates, bacteria were then labeled with BacLight Red, glycerol stocks were made and stored as described in Chapter 2.

Identification of immune cell subsets carrying *F. tularensis* after peripheral inoculation by flow cytometry

For the identification of immune cell subsets carrying *F. tularensis* after peripheral inoculation, perfused brains were placed in 3 ml of sterile HBSS without Ca^{+2} , and Mg^{+2} (Gibco) in a 5ml round bottom tube and were homogenized using a sterile Dounce homogenizer (10A/10B). Final volume was adjusted to 7 ml with HBSS. 3 ml ISP was added to make the brain homogenate 30% Percoll (GE Healthcare). In a 15 ml tube containing 70% Percoll, the brain homogenate-30% Percoll was slowly overlaid using a transfer pipette. This was centrifuged at 500xg for 30 minutes at room temperature without the brake on the centrifuge. After centrifuge, most of the top layer was vacuumed until 1 ml was left from the interface, the interface was then transferred on top of a 50 ml conical tube with a cell strainer. The cell strainer was washed by adding 10ml HBSS on top of the strainer, then centrifuged at 1,300 rpm for 10 minutes at 4°C. The pellet was resuspended with 1ml of staining buffer, then the cells counted. Cells were centrifuged at 1,300 rpm for 10 minutes at 4°C then resuspend in 100µl of FACS buffer in a 96-well round bottom plate. Fc shield was then added and incubated for 15 minutes at room temperature. 50µl of antibody master-mix (Figure 8a) was added and incubated for 30 minutes, then centrifuged for 2 minutes at 2,000 rpm. Cells were washed with 100µl of FACS buffer and centrifuged for 2 minutes at 2,000 rpm. Buffer was removed 100µl pre-warmed CytoFix/CytoPerm was added and incubated for 15 minutes. 200µl of 1x PermWash was added then plate centrifuged for 2 minutes at 2,000 rpm. Buffer was removed and cells resuspended with 100µl of master-mix cocktail of internal antibodies (Figure 8a), incubated for 20 minutes. 200µl of 1x PermWash was added and centrifuged the cells for 2 minutes at 2,000 rpm. Cell pellets were resuspended in 200µl

FACS buffer and transfer to 5ml round bottom tubes to analyze through flow cytometry using the Beckman Coulter Gallios at the Cytometry, Screening and Imaging Core Facility at the University of Texas at El Paso. Alternatively, antibody cocktail in Figure 8b were used then cell pellets were resuspended in 50µl FACS buffer and transfer to 1.5ml Eppendorf tubes, then samples were shipped to UT San Antonio for imaging flow cytometry as described in Chapter 2.

Suppression of macrophages in CD11b-DTR mice

CD11b-diphtheria toxin (DT) receptor (DTR) mice were injected with diphtheria toxin at 15ng/g in sterile PBS to selectively deplete blood and tissue macrophages 24 hours prior to LVS inoculation. CD11b-DTR mice were inoculated with 50µl of a 1×10^6 *BacLight* Red-labeled LVS suspension. Diphtheria toxin was then injected at 15ng/g in sterile PBS 24 hours following LVS inoculation then mice were harvested serially every six hours by perfusing with sterile PBS beginning at 42 hours post infection. Mice that had no toxin administered, were inoculated with *BacLight* Red-labeled LVS, and harvested at 48 hours post infection. C57BL/6 mice were inoculated with 50µl of a 1×10^6 *BacLight* Red-labeled LVS suspension and harvested at 42 hours post infection as a control group. Brain homogenate volume was then adjusted to 7 ml with HBSS. 3 ml ISP was added to make the brain homogenate 30% Percoll (GE Healthcare). In a 15 ml tube containing 70% Percoll, the brain homogenate-30% Percoll was slowly overlaid using a transfer pipette. This was centrifuged at 500xg for 30 minutes at room temperature without the brake on the centrifuge. After centrifuge, most of the top layer was vacuumed until 1 ml was left from the interface, the interface was then transferred on top of a 50 ml conical tube with a cell strainer. The cell strainer was washed by adding 10ml HBSS on top of the strainer, then centrifuged at 1,300

rpm for 10 minutes at 4°C. The pellet was resuspended with 1ml of staining buffer, then the cells counted. Cells were centrifuged at 1,300 rpm for 10 minutes at 4°C then resuspend in 100µl of FACS buffer in a 96-well round bottom plate. Fc shield was then added and incubated for 15 minutes at room temperature. 50µl of antibody master-mix (Table 3) was added and incubated for 30 minutes, then centrifuged for 2 minutes at 2,000 rpm. Cells were washed with 100µl of FACS buffer and centrifuged for 2 minutes at 2,000 rpm. Buffer was removed 100µl pre-warmed CytoFix/CytoPerm was added and incubated for 15 minutes. 200µl of 1x PermWash was added then plate centrifuged for 2 minutes at 2,000 rpm. Buffer was removed and cells resuspended with 100µl of master-mix cocktail of internal antibodies, incubated for 20 minutes. 200µl of 1x PermWash was added and centrifuged the cells for 2 minutes at 2,000 rpm. Cell pellet was resuspended in 200µl FACS buffer and transfer to 5ml round bottom tubes to analyze through flow cytometry.

Table 3. Flow Cytometry antibody panels for suppression of macrophages in CD11b-DTR mice
 Antibody panel used for flow cytometry performed at The University of Texas of El Paso using the Beckman Coulter Gallios at the Cytometry, Screening and Imaging Core Facility.

Antibody	Fluorophore
Iba-1	FITC
GFAP	PE
CD45	PE-CF594
B220	PerCP
BacLight	APC
CD11b	VioletFluor 450

***In vitro* Blood-Brain Barrier model**

To model the blood-brain barrier *in vitro*, we used 8.0 μ m PET membrane 24-well format cell culture inserts (Falcon) paired with 24-well plate (Falcon) to form a transwell setup (Figure 22). Complete growth media was added to both the top and bottom chambers for a total of 2ml. 5×10^5 Bend.3 cells (ATCC) were seeded and allowed to grow until an electrical resistance of 400-450 ohms was achieved (Figure 23). This was measured using a Millicell ERS-2 Epithelial Volt-Ohm Meter (Millipore). When the desired electrical resistance was achieved, a C57BL/6 mouse spleen was harvested into sterile 2 mL PBS, then using 5ml plunger to grind the tissue on a 70 μ m strainer on 50ml conical tube. When tissue was fully ground, the strainer was then rinsed with 5ml sterile PBS and centrifuged for 10 minutes at 1500 rpm. Pellet was then resuspended in ACK buffer (1.5 ml per spleen) and incubated at room temperature for 30 seconds, then added cell growth media directly without ciprofloxacin (1.5 ml per spleen). 5ml of PBS were then added and centrifuged for 10 minutes. The supernatant was then removed, and 3-5ml of media was then added. Trypan Blue was then used to count the cells, then centrifuged the cells at 300 \times g for 10 minutes, and the supernatant discarded. The cell pellet was then resuspended in 90 μ l of MACS buffer per 10^7 total cells. 10 μ l of CD11b MicroBeads UltraPure (Miltenyi) per 10^7 total cells were then added and mixed well then incubated for 10 minutes at 4°C. MACS buffer was then added to a final volume of 500 μ l for up to 5×10^7 cells. Then magnetic separation of CD11b⁺ cells was performed following manufacturer protocols. Briefly, MS column was placed in the magnetic field of a suitable MACS Separator and rinsed with the 500 μ l buffer. Cell suspension was added to the column and washed three times. The captured cells were eluted by removing the column from the magnet and flushed with 1ml of MACS buffer and the column plunger. A concentration of 5×10^5

macrophages per well were then infected with an MOI of 30 with pre-labeled *BacLight Red LVS*. Macrophages were then infected by incubating with pre-labeled LVS for 2 hours at 37°C. They were then washed with sterile PBS and centrifuged at 1,500 rpm for 10 minutes. Cells were then resuspended in a suspension of 60µl of gentamycin in 6ml complete media and incubated for 90 minutes at 37°C. During the last 30 minutes of incubation, DiO was added at 1:500 and DAPI at 1:1,1000. The cells were then washed with 5ml of sterile PBS and centrifuged at 1,500 rpm for 10 minutes. Cells were then resuspended in a suspension of 6µl of gentamycin in 6ml complete media. Bend.3 cells in the plate were then labeled by centrifuging at 1,500 rpm for 10 minutes then rinsed with 500µl sterile PBS. DAPI at 1:1,000 in complete media was then added to each well and placed on the belly dancer at RT for 30 minutes. The plate was then washed and centrifuged at 1,500 rpm for 10 minutes. Then media from each well was then replaced with 6µl:6ml gentamycin media. A concentration of 5×10^5 of infected and uninfected macrophages were then added to designated wells, 100 ng/mL MCP-1 (Tonbo) was also added to these same wells and plate was incubated for 24 hours at 37°C.

3.2 Results

Having observed a large population of peripheral macrophages infected by *BacLight Red* labeled LVS, we hypothesized that these macrophages may be importing LVS into the brain. Therefore, we sought to quantify the amount of bacterial fluorescence in various cell populations in the brain with the hypothesis that the highest bacterial infection load is likely to be the first cell type infected. For this, brain leukocytes were isolated by Percoll density gradient, stained with a cocktail of antibodies to identify cell types, and analyzed using the Beckman Coulter Gallios Flow

Cytometer in the Cytometry, Screening and Imaging Core Facility at the University of Texas at El Paso. Flow cytometry data showed an immune cell subset composition of the brain consisting of 13.6% peripheral macrophages, 5.9% microglia, 4.3% astrocytes, and 3.7% oligodendrocytes (Figures 17 and 18b). Of these immune cells, there is an immune cell distribution of LVS-positive cells as follows: 86.3% peripheral macrophages, 7.4% oligodendrocytes, 3.4% microglia, and 2.7% astrocytes (Figures 17 and 18a). Peripheral macrophages had a mean fluorescence intensity of 438 (Figures 16, 17 and 18c). When observing the mean fluorescent intensity of microglia, astrocytes, and oligodendrocytes the flow cytometry data shows that microglia had the second highest MFI following peripheral macrophages at 354, astrocytes followed with an MFI of 317, and oligodendrocytes had the lowest MFI of 306 (Figures 16, 17 and 18c).

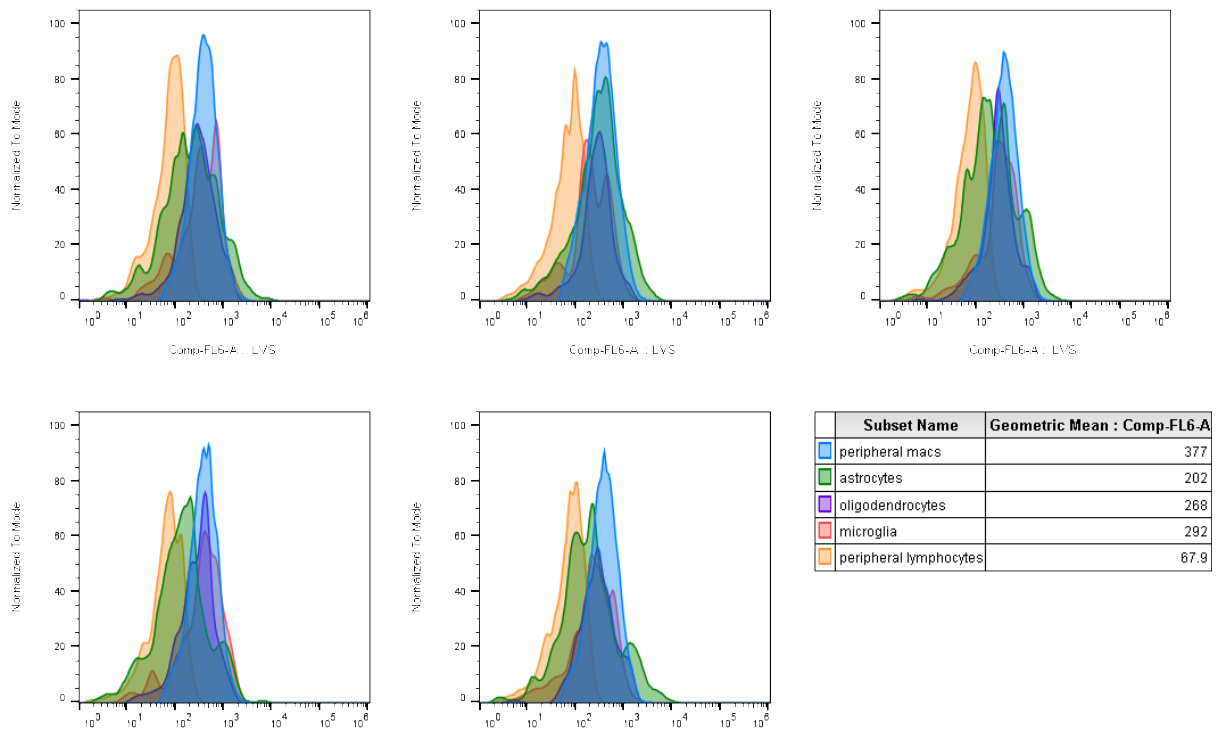


Figure 16. Populations of immune cells present in the brain after LVS neuroinvasion.

Immune cell subsets carrying *F. tularensis* after peripheral inoculation were identified with the use of flow cytometry. Leukocytes were isolated by Percoll density gradient from perfused animals and was followed by profiling of immune cell subsets by use of the Gallios Flow Cytometer from Beckman Coulter.

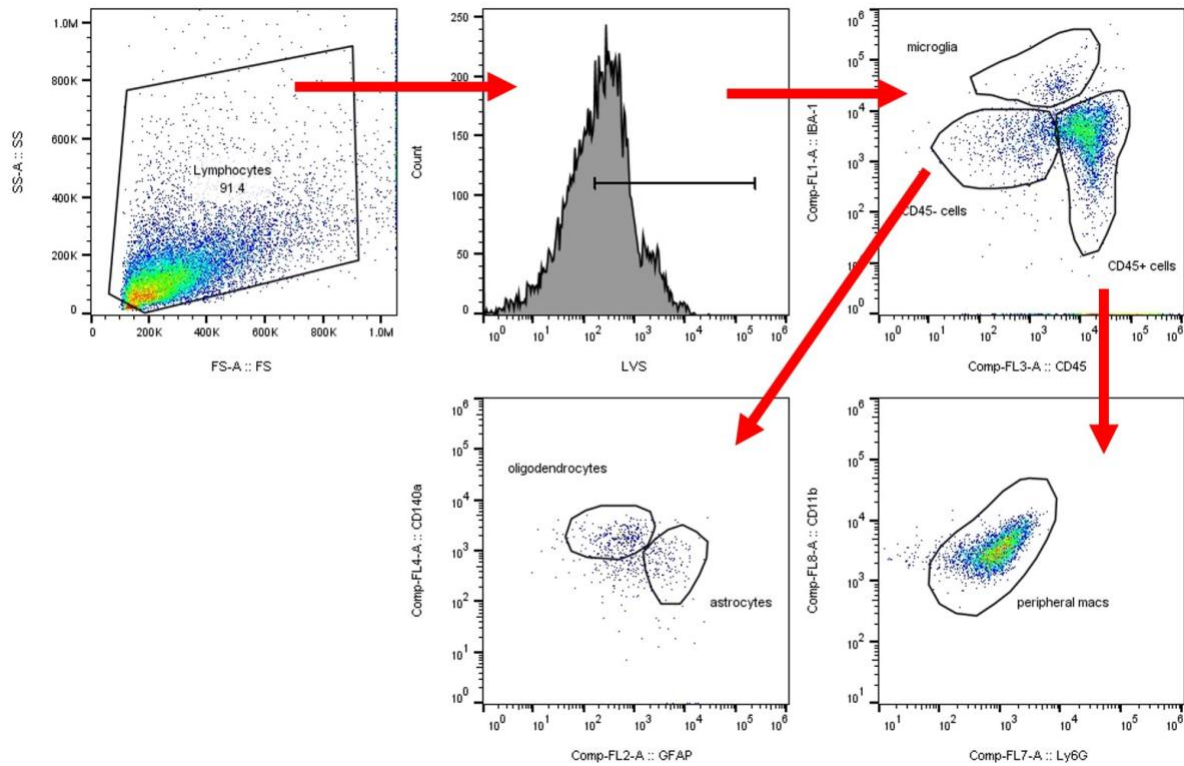


Figure 17. Immune cell subsets present in the brain after LVS neuroinvasion

Immune cell subsets carrying *F. tularensis* after peripheral inoculation were identified with the use of flow cytometry. Leukocytes were isolated by Percoll density gradient from perfused animals and was followed by profiling of immune cell subsets by use of the Gallios Flow Cytometer from Beckman Coulter.

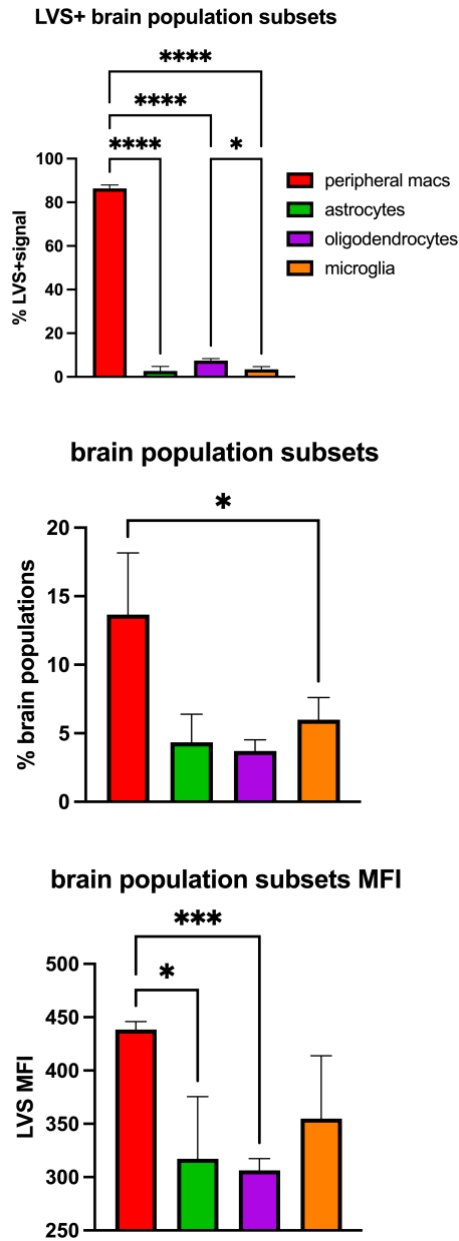


Figure 18. Immune cell subsets present in the brain after LVS neuroinvasion

Immune cell subsets carrying *F. tularensis* after peripheral inoculation were identified with the use of flow cytometry. Leukocytes were isolated by Percoll density gradient from perfused animals and was followed by profiling of immune cell subsets by use of the Gallios Flow Cytometer from Beckman Coulter.

To confirm this result and visualize the bacterial load, isolated leukocytes were stained with antibody cocktail and shipped to the University of Texas at San Antonio for analysis on the Amnis ImageStream Imaging Flow Cytometer in the Biophotonics Core Facility. These data recapitulate prior observations of microglial and astrocyte infection but also demonstrate substantial levels of infection in peripheral macrophages (Figure 19). These data suggest that peripheral macrophages may have been infected in the periphery and then migrated into the brain parenchyma carrying with them the LVS.

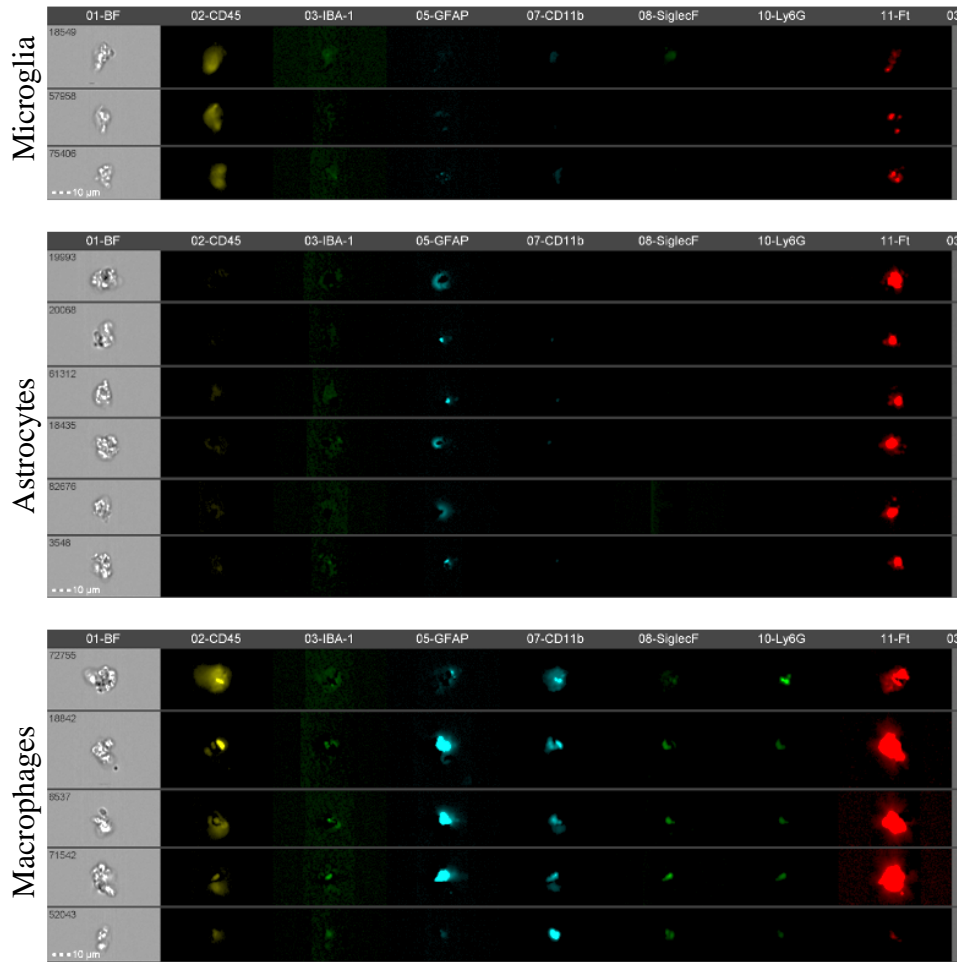


Figure 19. Immune cells present in the brain after LVS infection captured by imaging flow cytometry

Immune cell subsets carrying *F. tularensis* after peripheral inoculation were identified with the use of imaging flow cytometry. Leukocytes were isolated by Percoll density gradient from perfused animals and was followed by profiling of immune cell subsets in collaboration with UT San Antonio by use of the Amnis ImageStream X imaging flow cytometer.

If this hypothesis is correct, then depleting peripheral macrophages should prevent LVS from entering the brain. To answer this question, we used CD11b-diphtheria toxin (DT) receptor (DTR) transgenic mice where the administration of DT selectively depletes blood and tissue macrophages. CD11b-DTR mice were administered 15ng/g of DT 24 hours prior to LVS inoculation. Mice were then inoculated with 50 μ l of a 1x10⁶ *BacLight* Red-labeled LVS suspension, and 15ng/g of DT was again administered 24 hours following LVS inoculation, then harvested every 6 hours starting at 42 hours post infection. Mice that had no toxin administered, were inoculated with *BacLight* Red-labeled LVS, and harvested at 48 hours post infection. Single cell brain homogenates were stained with antibody cocktail as shown in Table 3.

C57BL/6 mice infected with LVS showed a strong LVS signal and CD45⁺CD11b⁺ macrophages, and microglia (Figure 20). LVS-infected CD11b-DTR mice without toxin administered had a strong presence of peripheral macrophages and microglia, as well as a strong bacteria signal (Figure 21). However, prior administration of diphtheria toxin to CD11b-DTR mice resulted in an elimination of macrophages from the brain and resulted in no *BacLight* Red bacterial signal in any cell type (Figure 22). In addition, no bacterial growth was recoverable on modified Mueller-Hinton plates (data not shown). These data demonstrate that peripheral macrophages are necessary for the entrance of LVS into the brain and its dissemination to other cell types.

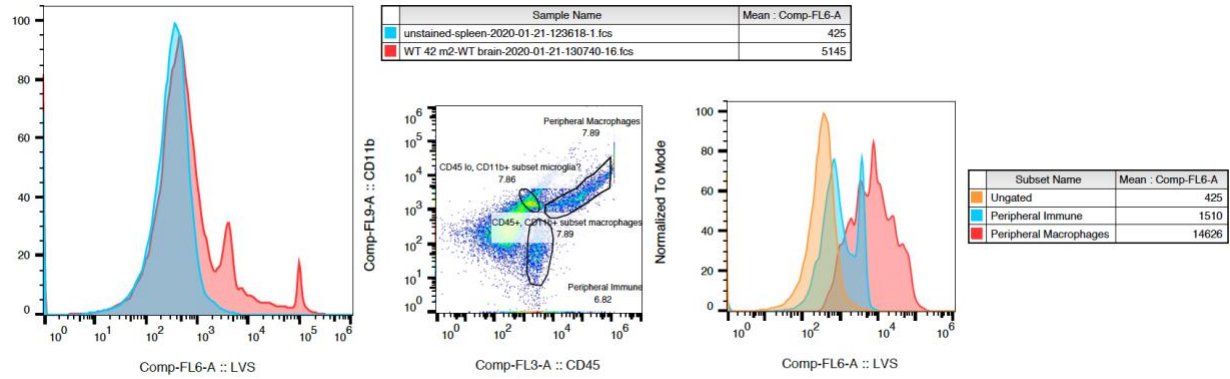


Figure 20. C57BL/6 mice LVS infected.

C57BL/6 mice were inoculated with 50 μ l of a 1x10⁶ BacLight Red-labeled LVS suspension and harvested at 42 hours post infection as a control group. Mice were perfused, their brains were harvested, homogenized, and plated for CFUs. Tissue homogenates were then used to isolate leukocytes to label for Iba1, GFAP, CD45, and CD11b antibodies and analyzed through flow cytometry.

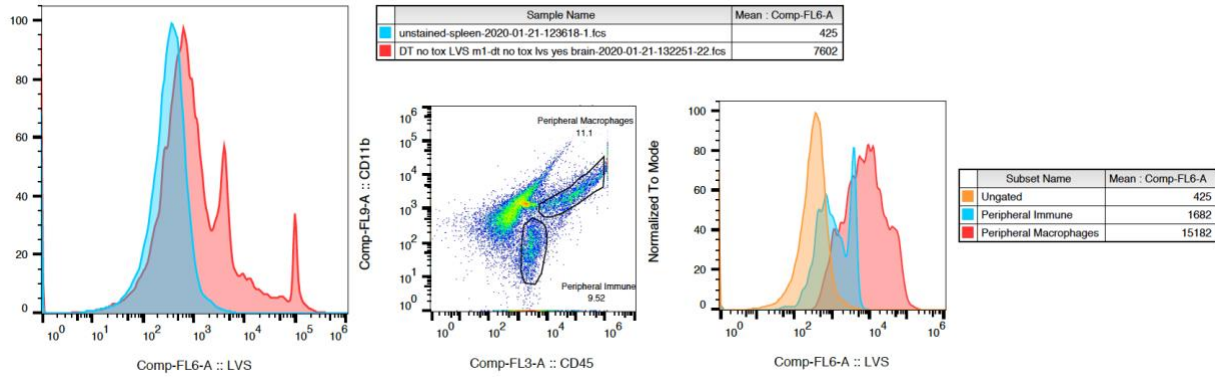


Figure 21. CD11b-DTR mice without toxin administered

CD11b-DTR mice without toxin administered, were inoculated with 50 μ l of a 1x10⁶ *BacLight* Red-labeled LVS, and harvested at 48 hours post infection. Mice were perfused, their brains were harvested, homogenized, and plated for CFUs. Tissue homogenates were then used to isolate leukocytes to label for Iba1, GFAP, CD45, and CD11b antibodies and analyzed through flow cytometry.

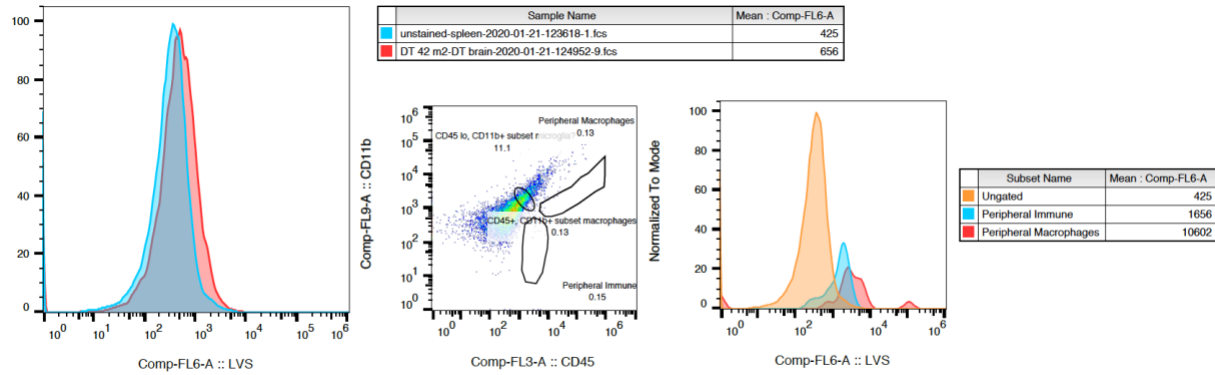


Figure 22. CD11b-DTR mice with diphtheria toxin administered

CD11b-DTR mice were administered 15ng/g of DT 24 hours prior to LVS inoculation. Mice were then inoculated with 50µl of a 1×10^6 *BacLight* Red-labeled LVS suspension, and 15ng/g of DT was again administered 24 hours following LVS inoculation, then harvested every 6 hours starting at 42 hours post infection. Mice were perfused, their brains were harvested, homogenized, and plated for CFUs. Tissue homogenates were then used to isolate leukocytes to label for Iba1, GFAP, CD45, and CD11b antibodies and analyzed through flow cytometry.

There are three mechanisms recognized for the invasion of microorganisms across the blood-brain barrier, paracellular (between endothelial cells), transcellular (through endothelial cells), and transmigration otherwise known as “Trojan horse” where it is carried in by macrophages. Our data suggests that the dominated mechanism used by *F. tularensis* to invade the CNS is the Trojan horse.

To demonstrate that *F. tularensis*-infected macrophages can transmigrate across the blood-brain barrier, we utilized an *in vitro* model of the blood-brain barrier. Bend.3 endothelial cells were cultured in cell culture inserts with 8.0 μ m pores to allow cell migration (Figure 23). The transendothelial electrical resistance (TEER) was monitored until the growing cells plateaued at an electrical resistance of 400-450 Ω , or 75-90 Ω cm², indicative of a complete monolayer (Figure 24). Macrophages were purified from C57BL/6 mouse spleens using CD11b-magnetic microbeads, infected with LVS and stained with DiO, for identification, prior to addition to the transwell plate. Labeled infected or uninfected macrophages were then added alone or with MCP-1 in the lower chamber to induce migration and incubated for 24 hours at 37°C. It was observed that at 24 hours of incubation there was a significant migration of infected macrophages when compared to uninfected macrophages (Figure 25a). When comparing migration of infected and uninfected macrophages, it was consistent that with and without MCP-1 infected macrophages had a greater migration number than their uninfected counterparts (Figure 25b). However, it is evident that in the presence of MCP-1 macrophage migration is radically improved.

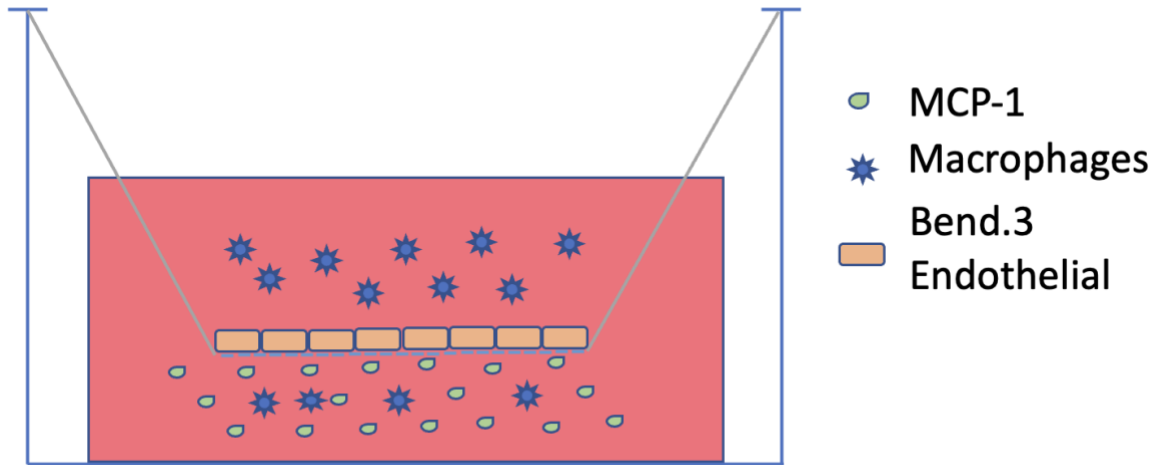


Figure 23. Representation of a Transwell

Digital representation of a cross-section of a Transwell insert. A monolayer of Bend.3 endothelial cells were first grown on an 8.0 μ m microporous membrane, then 5×10^5 macrophages were added to the insert (top chamber), followed by 100 ng/mL of MCP-1 to the bottom chamber. This was incubated for 24 hours at 37°C.

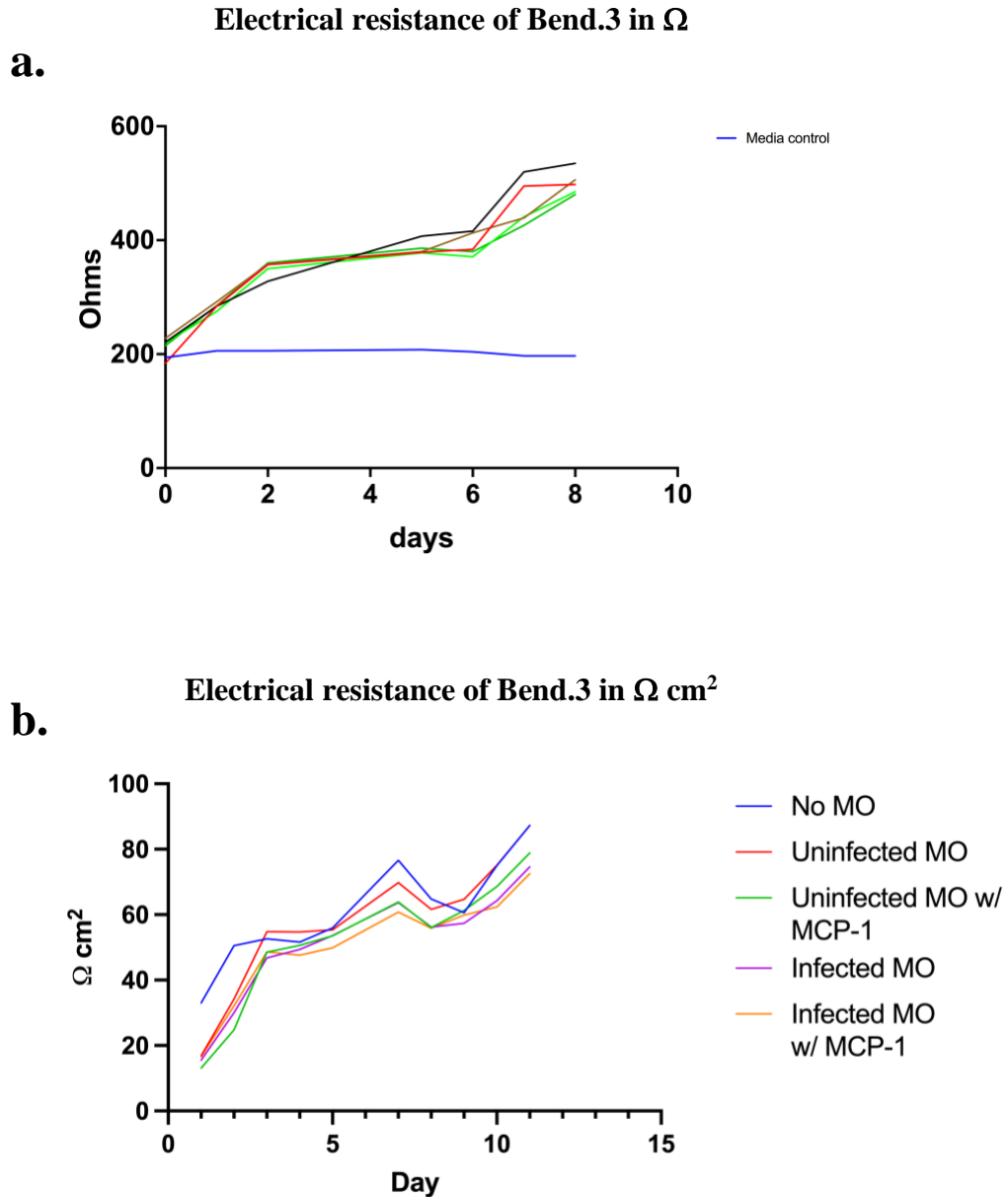


Figure 24. Electrical resistance of Bend.3 cells in Transwells using TEER

F. tularensis translocation via the Trojan Horse pathway using Transwell migration assay. 8.0 μm cell culture inserts were paired with 24-well plates to form a Transwell assay. Bend.3 cells were seeded at 5×10^5 cells/well and allowed to proliferate until an electrical resistance of (A) 400-450 ohms had been reached, or (B) 75 -90 $\Omega \text{ cm}^2$, indicative of a complete monolayer.

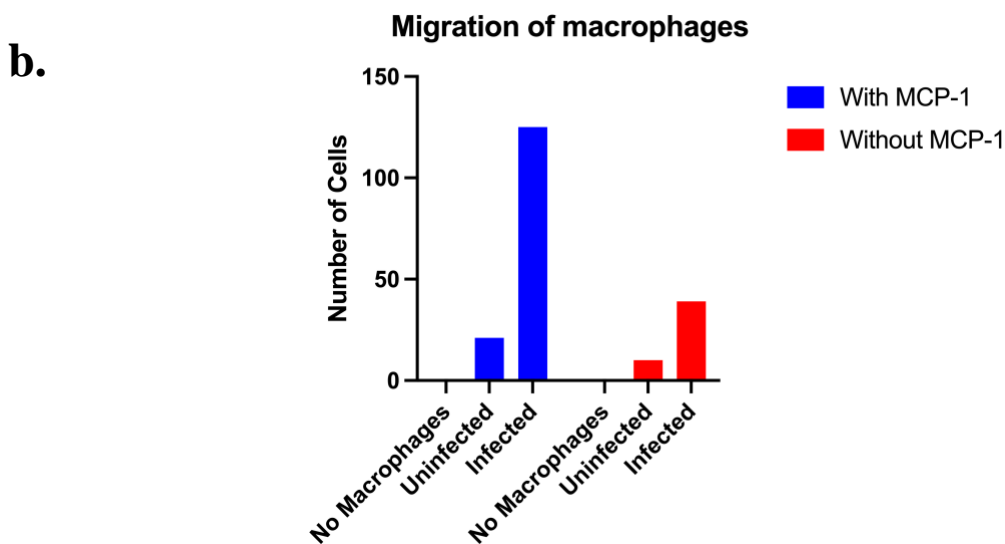
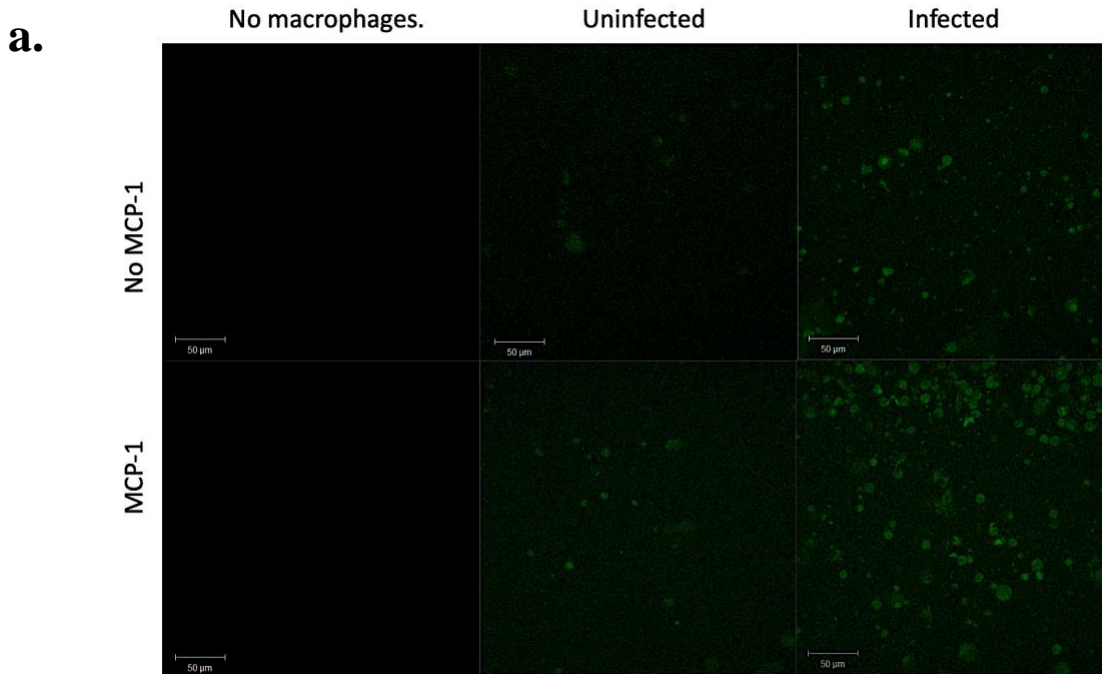


Figure 25. Migration of macrophages.

(A) C57BL/6 mouse spleens were harvested and CD11b⁺ cells were isolated using magnetic microbeads. 5×10^5 macrophages were then infected with an MOI of 30 with pre-labeled *BacLight Red LVS*. Macrophages were then stained with DiO. 100ng/mL MCP-1 was then added, and plate incubated for 24 hours at 37°C, and imaged with confocal microscopy.

(B) Quantitation of migration of infected and uninfected macrophages with MCP-1 (blue), and without MCP-1 (red).

3.3 Discussion

This study is the first demonstration that *F. tularensis* LVS can productively infect the brain. We have identified the bacterial burden of different cell populations and elucidated the mechanism by which *F. tularensis* traverses the blood-brain barrier. Our data showed that the highest level of bacterial burden of immune subsets in the brain was in peripheral macrophages. This suggested that peripheral macrophages may be carrying LVS into the brain. Indeed, depletion of macrophages resulted in elimination of bacteria in the brain. Furthermore, purified infected macrophages demonstrated a high level of transit across an *in vitro* endothelial blood-brain barrier model.

Profiling of immune cell subsets carrying *F. tularensis* after peripheral inoculation was done by use of the Gallios Flow Cytometer from Beckman Coulter. These data suggest that *F. tularensis* has a higher affinity to target macrophages than astrocytes, oligodendrocytes, and microglia. It cannot be discarded that infected macrophages from the periphery are crossing into the brain in large quantities due to a compromised BBB because of the inflammation levels happening after infection. This would warrant further studies of the BBB after infection with *F. tularensis* to see if a leaky or otherwise compromised BBB is occurring due to the high inflammation levels seen following infection.

Identification of immune cell subsets carrying *F. tularensis* after peripheral inoculation with the use of imaging flow cytometry show that CD45⁺Cd11b⁺ macrophages have the largest visualized APC signal for LVS. Gating for GFAP⁺ astrocytes also showed APC positive cells shouldering some bacterial load. Finally, CD45⁺IBA-1⁺ microglia were also confirmed to be targeted by LVS and carry some bacteria burden. These data confirm our flow cytometry findings from Chapter 2 suggesting macrophages are shouldering the majority of the LVS burden after

infiltration. Astrocytes are observed to shoulder some bacteria burden, as are microglia cells and oligodendrocytes are detected to have the lesser LVS load. These data confirm our findings from our flow cytometry study suggesting that macrophages are largely more targeted by *F. tularensis* than astrocytes, microglia, or oligodendrocytes. Again, it cannot be discarded that infected macrophages from the periphery are crossing into the brain in large quantities due to a compromised BBB because of the high inflammation levels happening after infection. This further supports a need for further studies of a possibly leaky or otherwise compromised BBB due to the high inflammation levels seen following infection.

To elucidate *F. tularensis* translocation via the Trojan Horse pathway in an *in vitro* model that is widely used to study the BBB was used to form a transwell assay. It was observed that at 24 hours of incubation there was a significant migration of infected macrophages when compared to uninfected macrophages. When comparing migration of infected and uninfected macrophages, it was consistent that with MCP-1 infected macrophages had a greater migration number than their uninfected counterparts. Transwell assays have been largely accepted as an *in vitro* model of the BBB. Although there are many possible models of a Transwell migration assay, such as co-cultures with microglia, astrocytes, and neurons, our search for an adequate model proved to be much more difficult than expected. We tried a co-culture of Bend.3 cells and astrocytes, however that model did not work for us. The astrocyte cell line we used was slower to proliferate than the Bend.3 cells and would therefore pose a timing discrepancy when trying to achieve an optimum environment ready for macrophage infection. Unfortunately, we were not able to perform a migration assay using the astrocyte/Bend.3 co-culture as the resistance readings were consistently too low, and the astrocyte cells would often go to the bottom chamber. In time, we decided it was best to continue with only a Bend.3 endothelial cell culture, and it was this that gave us the best results. This in

itself poses a limitation to our experimental model as it is not a method involving a co-culture of astrocytes, microglia, or neurons, furthermore, it includes the use of serum in the cell medium and is used as an additional chemoattractant to MCP-1, a chemoattractant itself. This study is not intending to state a claim that MCP-1 is a recruiting cytokine in the brain, however, we know that MCP-1 recruits macrophages experimentally and as such we used it in our *in vitro* experiment.

In the initial stages of this experiment, we tried using a C57BL/6 macrophage cell line, the cell proliferation rate was about equal to that of the Bend.3 cell line, and the migration of infected and uninfected macrophages observed after staining but before washing was excellent. However, after washing the plate there was an incredibly high amount of cell loss. This was troubleshooted in many ways, until the use of isolated mouse macrophages was suggested, which is the method that best worked for us. The next optimization complication we faced was in successfully staining both Bend.3 and macrophages. At first, we tried anti-CD45 to label macrophages and anti-CD31 to label Bend.3 cells, however, that also did not work for us. The antibody staining would not offer clear delineation of cells and would often result in a lot of background when trying to image with the confocal microscope. We tried different methods and optimizations for using these antibodies, until we decided on optimizing lipophilic tracer DiO to label macrophages which finally worked for us.

We then asked if we could suppress macrophages after infection. C57BL/6 mice infected with LVS and harvested 42 hours post infection showed a strong presence of CD45⁺CD11b⁺ macrophages and APC signal. CD11b-DTR mice without toxin administered, LVS infected, harvested 48 hours post infection, like the WT mice, showed a strong presence of CD11b⁺ cells to include macrophages and microglia, and APC signal. It was observed in CD11b-DTR that when toxin is administered followed by LVS infection, as soon as 42 hours post infection, the CD11b⁺

cells are entirely depleted, as well as an absent LVS APC signal. These data support our Transwell assay findings suggesting a transmigration, or “Trojan Horse” type mechanism being used by *F. tularensis* to traverse the BBB. The ability to deplete tissue CD11b⁺ cells in an infected model enables us to confirm our previous findings. Indeed, peripheral macrophages repopulate in the CD11b-DTR mouse model after withdrawal of DT, however, this drawback could be resolved using a complete macrophage knockout mouse model. This study also opens the question for *F. tularensis*’ use of alternative mechanisms for traversing the BBB as is the case with *L. monocytogenes* and *M. tuberculosis*. Each of these two pathogens use a transmigration or “Trojan Horse”, and paracellular mechanisms to cross the BBB, and as mentioned in Chapter 2, other studies have demonstrated that these two bacteria are capable of infecting both microglia and astrocyte cells thereby sharing some similarities [89-91].

This study has demonstrated that *F. tularensis* LVS crosses the blood-brain barrier by the “Trojan Horse” mechanism, and that it productively infects the brain parenchyma by targeting microglia, astrocytes, and oligodendrocytes in addition to the overwhelming bacterial burden present from peripheral macrophages. The inducement of *F. tularensis* to cross the BBB remains to be elucidated, however, as this study has demonstrated, LVS has the capability to infect microglia, astrocytes, and oligodendrocytes, furthermore, the likelihood of other cell types being targeted by this bacterium cannot be discarded. Moreover, it would be compelling to explore the motive an LVS-infected macrophage would have to transmigrate into the CNS.

Chapter 4: Analyze the neuroinflammatory response after intradermal inoculation with LVS

4.1 Materials and Methods

All animal procedures were carried out in accordance with the Guide for the Care and Use of Laboratory Animals [86] and approved by the Institutional Animal Care and Use Committee of the University of Texas at El Paso. Male C57BL/6 mice between six to eight weeks old were used in all studies, they were bred and maintained as described in Chapter 2. For intradermal injection, mice were anesthetized with 3-5% isoflurane and injected intradermally in the flank above the hindquarters with 1×10^6 pre-labeled LVS bacteria suspension using sterile PBS in a volume of 50 μ l. Animals were monitored and evaluated for clinical symptoms of disease as described in Chapter 2. All animals were humanely euthanized per the American Veterinary Medical Association standards and organ harvest was performed 72 hours post-infection, unless otherwise noted. Once an animal was euthanized, its chest cavity was exposed, and a blunt needle was inserted into the heart through the left ventricle towards the aorta and clamped into place. Sterile PBS was then used to perfuse the animal until its vasculature was apparently cleared of blood. The brain was removed from the skull and placed in sterile PBS for immediate use, or in *RNAlater* and stored at 4°C.

F. tularensis holarctica (LVS) was obtained from Denise Monack (Stanford University) and was grown on chocolate agar plates, bacteria were then labeled with *BacLight Red*, glycerol stocks made and stored as described in Chapter 2.

Determine general neuroinflammatory response in the mouse brain after peripheral intradermal inoculation with LVS

Mice were infected and brains harvested into 1mL of sterile PBS. Total brain tissue was homogenized using a sterile Dounce homogenizer (10A/10B). The homogenate was centrifuged for 10 minutes at 1,500 rpm to pellet the cells. The supernatant was removed for analysis to represent the extracellular secreted environment within the brain parenchyma. Concentrations of IL-1 β , IL-2, IL-6, IFN- γ , IL-12p70, TNF- α , IL-22, IL-23, IL-17A, IL-27, GM-CSF, IL-18, IL-10, IL-4, IL-5, IL-9, and IL-13 in the parenchyma of infected and control animals were determined by multiplex ELISA (MilliPlex, Millipore Sigma) and analyzed on a Luminex MagPix following manufacturer's protocols. 200 μ L of Wash buffer was placed into each well, the plate was then sealed and placed on a shaker for 10 minutes at room temperature. Wash buffer was removed by inverting the plate and tapping it onto paper towels. 25 μ L of Standard or Control were then added to the appropriate wells, Assay buffer was used for 0pg/mL standard (background). 25 μ L of Assay buffer was added to each sample well. 25 μ L of matrix solution was added to the background, Standards, and Control wells. 25 μ L of sample was then added into the appropriate wells. 25 μ L of beads were then added to each well while mixing well intermittently to avoid settling. The plate was sealed and wrapped in foil then incubated on a shaker overnight (16-18 hours) at 4°C. Using a handheld magnet, well contents were removed, and plate was washed two times. 25 μ L of Detection antibodies were added to each well, the plate was sealed, covered with foil, and incubated at room temperature on a shaker for 1 hour. 25 μ L of Streptavidin-Phycoerythrin was then added to each well containing detection antibodies. The plate was then sealed, covered with foil, and incubated on a shaker at room temperature for 30 minutes. Again, using a handheld magnet plate holder, well

contents were removed and the plate was washed two times. 150µL of sheath fluid was then added to all wells, plate was sealed, covered, placed on a shaker and beads were resuspended for 5 minutes. The plate was then run on a Luminex MagPix instrument. Analysis was completed by ANOVA with post-hoc and Mann-Whitney U test.

Determine regional neuroinflammatory response in the mouse brain after peripheral intradermal inoculation with LVS

Brains of infected and uninfected mice were harvested and collected into RNA^{later} and stored at 4°C. An Adult Mouse Brain Slicer matrix (Zivic Instruments) was used to cut every 1.5mm and yield eight slices from the rostral to caudal direction that were collected into 1mL of Trizol (Invitrogen) and 1cm of 1.0mm zirconia/silica beads (BioSpec Products). The tissue was disrupted using a bead beater for 1 minute, then homogenates were transferred to a microcentrifuge tube and allowed to rest for 5 minutes at room temperature. 200µL chloroform was then added to the tube making sure the cap was secured then shook it vigorously for 15 seconds. The tube was allowed to rest again for 3 minutes at room temperature. Then it was centrifuged at 12,000 x g for 15 minutes at 4°C. The upper aqueous phase was then transferred to a new tube. 600µL of 70% ethanol was added and mixed thoroughly by vortexing. 700µL of the sample was transferred to an RNeasy lipid mini spin column (Qiagen) and placed in a 2mL collection tube. Closed the lid then centrifuged for 15 seconds at 8,000 x g at room temperature. Flow through was discarded. The remainder of the sample was added to the column, then centrifuged for 15 seconds at 8,000 x g at room temperature. Flow through was discarded. 700µL of buffer RW1 was added to the RNeasy Mini spin column, then centrifuged for 15 seconds at 8,000 x g. Flow through was discarded.

500 μ L of buffer RPE was added to the column then centrifuged for 15 seconds at 8,000 x *g*. Flow through was discarded. The same step was repeated, 500 μ L of buffer RPE was added to the column then centrifuged for 2 minutes at 8,000 x *g*. Flow through was discarded. The column was placed in a new 2 mL collection tube and the old collection tube was discarded with the flow through. This was centrifuged for 1 minute at maximum speed. The column was then placed in a new 1.5 mL collection tube and 50 μ L of RNase-free water was added directly to the spin column membrane. The column was centrifuged for 1 minute at 8,000 x *g*. This step was repeated, 50 μ L of RNase-free water was added directly to the spin column membrane. The column was centrifuged for 1 minute at 8,000 x *g*. The collected RNA was frozen at -80°C until further use. To quantify the RNA, a NanoDrop One (Thermo Scientific) was used. 1 μ L of RNase-free water was used to blank the NanoDrop, then each RNA sample was quantified with 1 μ L as well. mRNA quantitation by qRT-PCR was performed with Cybrfast 1-Step RT-qPCR Hi-ROX kit (Tonbo), IL-1 β and IL-6 primers (Millipore Sigma) in a StepOne Real-Time PCR System (Thermo Fisher Scientific). The data were normalized against tubulin controls, Δ Ct values were then used to calculate $2^{-\Delta$ Ct as a measure of mRNA expressed in each sample, this value was then used to calculate the quantitative relation between infected and uninfected samples.

4.2 Results

To determine the general neuroinflammatory response in the mouse brain following infection with *F. tularensis*, concentrations of immune cytokines were determined by multiplex ELISA and analyzed on a Luminex MagPix following manufacturer's recommended protocol. Analysis was completed by ANOVA with post-hoc Mann-Whitney U test. Of the cytokines tested, the inflammatory cytokines IL-6, IL-1 β , IFN- γ , and TNF- α (Figure 25) all had significantly higher levels of expression when compared with uninfected samples, *p < 0.05. IL-6 had a mean expression of 3620 pg/mL when compared to its baseline of 25 pg/mL. IL-1 β had a mean expression of 24 pg/mL and its baseline expression was 9pg/mL. IFN- γ had a mean expression of 407 pg/mL when compared to a baseline expression of 7 pg/mL. TNF- α had a mean expression of 53 pg/mL while its baseline expression was 5 pg/mL. The induced secretion of these cytokines in response to LVS invasion of the brain represents a neuroinflammatory response to the presence of the bacteria.

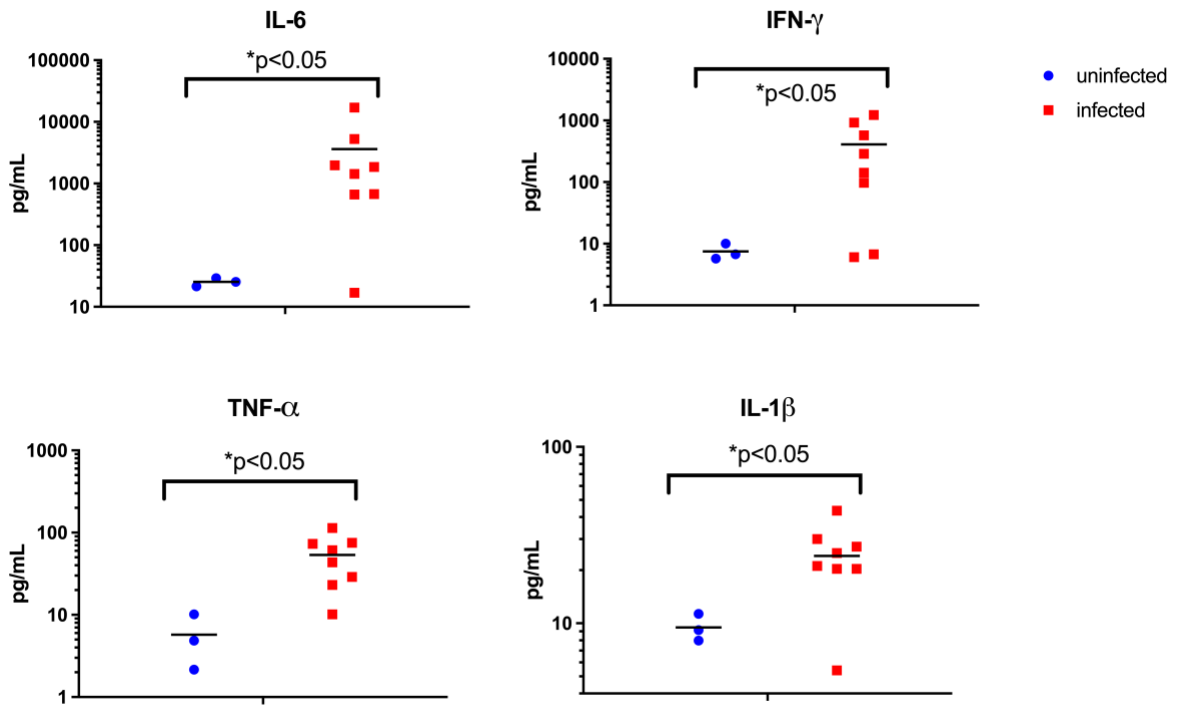


Figure 26. Inflammatory cytokines of whole brain produced in the mouse brain after LVS infection.

Concentrations of different markers in infected and control animals were determined by multiplex ELISA and analyzed on a Luminex MagPix following manufacturer's protocols.

Knowing that immune cells in the brain are responding to the presence of the bacteria by secreting inflammatory cytokines in total brain homogenates, we sought to determine how widespread was the neuroinflammatory response. To determine whether inflammatory responses existed in subregions of the mouse brain following infection with *F. tularensis*, brains of infected and uninfected mice were harvested and collected into RNAlater. An Adult Mouse Brain Slicer matrix was then used to cut in the rostral to caudal direction every 1.5mm to yield eight slices. Expression of IL-1 β and IL-6 mRNA was quantified by qRT-PCR and normalized against tubulin controls. Ct values were then used to calculate $2^{-\Delta Ct}$ as a measure of mRNA expressed in each sample, this value was then used to calculate the quantitative relation between infected and uninfected samples.

Overall, there were regional differences in the expression of IL-1 β and IL-6. We observed that slices 4, 5, and 6 have a trend for higher of expression of IL-1 β in infected tissues when compared to the uninfected controls (Figure 27). When looking at the same quantitative relation for IL-6, we observed that in slices 3 and 4 there was a definite trend for increased expression when compared to the uninfected controls. It is interesting that the expression of IL-1 β is more caudal while the expression of IL-6 is further rostral. Since IL-1 β is the cytokine that initiates the inflammatory process and IL-6 is an effector cytokine, this may suggest that the bacteria initially invade the brain towards the hindbrain.

Comparison of approximate coordinates of these slices to a sagittal representation of a mouse anatomical brain map allows us to hypothesize the brain regions that might be most affected by bacterial invasion and response (Figure 28). It is important to note the olfactory bulb was not part of our studies, and has therefore been excluded from the representation in Figure 28.

Furthermore, the Zivic Instruments Adult Mouse Brain Slicer is highly precise as it is measured to have 500 μ m coronal section slice intervals, therefore allowing for reproducible results. As depicted in Figure 28, Slice 3 (S3) mainly contains cerebral cortex, thalamus, and hypothalamus. Slice 4 (S4) contains cerebral cortex, hippocampus, thalamus, hypothalamus, and midbrain. Slice 5 (S5) is mainly composed of midbrain and pons, in addition to some hypothalamus tissue. Finally, Slice 6 (S6) is composed of midbrain, pons, cerebellum, and medulla. In these regions, neurons, astrocytes, microglia, and endothelial cells all produce IL-6 under normal conditions [74]. However, when facing stress such as that from an infection, large amounts of IL-6 will be secreted, especially when stimulated by IL-1 β [92].

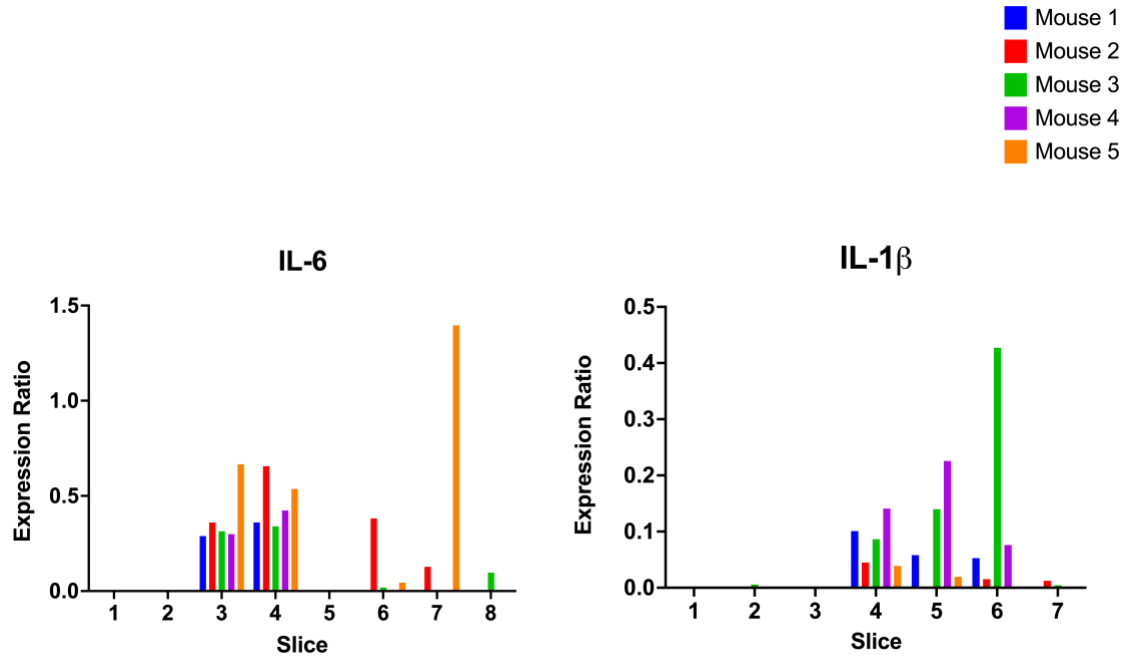


Figure 27. IL-6 and IL-1 β quantitative relation between infected and uninfected samples

An Adult Mouse Brain Slicer matrix was used to cut in the rostral to caudal direction every 1.5mm to yield eight slices. Using a RNeasy Lipid Tissue kit, RNA was isolated and mRNA was then quantitated by qRT-PCR on a StepOne Real-Time PCR System. The data were normalized against tubulin controls. ΔCt values were then used to calculate $2^{-\Delta\text{Ct}}$ as a measure of mRNA expressed in each sample, this value was then used to calculate the quantitative relation between infected and uninfected samples.

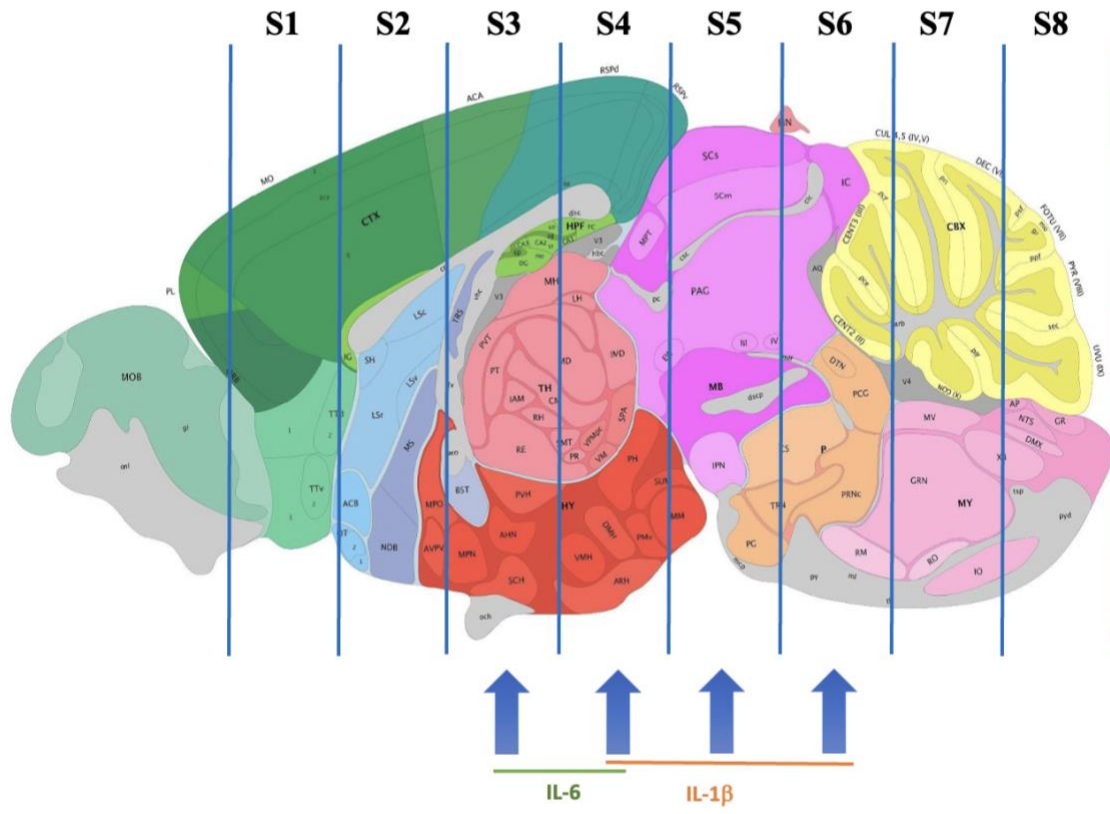


Figure 28. Sagittal image representation of mouse anatomical brain slices

Sagittal image representation of a mouse anatomical brain regions and overlay of approximate coordinates slices were made with the Zivic Instruments Adult Mouse Brain Slicer 500µm matrix. Slices were made every 1.5 mm yielding 8 slices. Base image extracted from Allen Brain Atlas.

4.3 Discussion

Our study has confirmed an active inflammatory response in the CNS following peripheral inoculation. We have surveyed general and regional brain tissue inflammation with multiple markers classically indicative of an inflammatory response. These data demonstrated that the migration of *F. tularensis* into the brain was recognized as an invasion initiating the inflammatory response of immune cells in the brain. This is the first demonstration of a productive brain infection by *Francisella tularensis*.

General inflammation following *F. tularensis* infection was identified by the use of a multiplex ELISA where concentrations of IL-1 β , IL-6, IFN- γ , and TNF- α were analyzed. It was detected that IL-6, IL-1 β , IFN- γ , and TNF- α (Figure 25) all had significantly higher levels of expression when compared to their baselines. As previously mentioned, when facing stress such as that from an infection, large amounts of IL-6 will be secreted, especially when stimulated by IL-1 β [92]. Bacterial pathogens such as *F. tularensis*, typically induce IL-6 in astrocytes and microglia [92], IFN- γ also induces secretion of IL-6 in microglia cells lines [93, 94], however, in contrast to IFN- γ , TNF- α promotes IL-6 in astrocytes but not microglia [95].

Regional inflammation following *F. tularensis* infection was identified by the use of an Adult Mouse Brain Slicer matrix. Slices were made in both infected and uninfected controls in the rostral to caudal direction every 1.5mm to yield eight slices. mRNA was quantitated by qRT-PCR, and expression of IL-1 β and IL-6 was analyzed. The data concluded that in more rostral-located Slices 3, and 4 for every mouse sampled there is a definite trend for increased expression of IL-6,

an effector cytokine. When looking at the same quantitative relation, it is observed that Slices 4, 5, and 6, encompassing part of the hindbrain, have a higher trend of expression for IL-1 β , an initiating cytokine. These data may suggest that peripheral macrophages are initially transmigrating through a place located in the hindbrain to later invade other brain regions. Indeed, there is a spread of the inflammatory response, it would be compelling to explore the distribution of *F. tularensis* within the brain, and in conjunction study the corresponding spread of inflammation. The resulting inflammation from *F. tularensis* neuroinvasion could lead to damage to neurons and other cells in these regions, therefore, it is possible that cognitive or behavioral disorders arise following infection and thus should be explored.

The area postrema is a circumventricular organ that is located at the caudal part of the fourth ventricle, is a single midline structure, is highly vascularized, and is associated with the vagus nerve. It also is highly involved in the emesis response, fluid balance, feeding and metabolism, and in the immune response [96-100]. The area postrema capillaries, unlike the capillaries in the brain parenchyma, lack the expression of tight junction proteins such as claudin-5, claudin-12, and occludin [101]. However, there are neuron and glia cells present in the area postrema such as astrocytes, oligodendrocytes, microglia, and macrophages that consistently patrol the area [102-104]. Both astrocytes and microglia in the area postrema express TLR4 which leads to the activation of proinflammatory cytokines [105]. Furthermore, microglia and macrophages exposed to LPS in rats have shown higher expression of IL-1 β [100]. The involving of the sensing mechanism is not yet understood; however, we have shown that infected macrophages can cross the blood-brain barrier.

Under normal conditions, neurons astrocytes, microglia, and endothelial cells all produce IL-6, IL-1 β is also produced by astrocytes and microglia under normal conditions, however, when cells are facing stress such as that from an infection by *F. tularensis*, large amounts of IL-6 will be secreted due to stimulation by IL-1 β upregulation [74, 92]. IL-1 β is therefore an important mediator of inflammation particularly in the hypothalamus and hippocampus [106]. In the case of *L. monocytogenes*, studies demonstrated that infected tissue from wild-type mice showed localization of inflammation in the lateral ventricles and in the periventricular brain stem [87].

Though the Adult Mouse brain slicer matrix is calibrated to have 500 μ m intervals for slicing and is, therefore, highly precise in producing equal slices of tissue it does represent an opportunity for user error due to the close proximity of the “teeth” for each slice. This close proximity results in a situation where the user must have excellent eyesight and an ability to keep track of which slot has been used already and which is next for slicing. Another difficulty in using the slicer matrix is the brain tissue can at times slide around the matrix and repositioning to its original location is quite a challenge. Given that the slices are quite thick at ~1.5mm each, it would not be possible to use a microtome or similar instrument to produce such thick slices. The only alternative that comes to mind would be to employ multiple blades and not withdraw them from the matrix until all slices have been made.

Chapter 5: Overview and final conclusions

Tularemia meningitis is a rare zoonotic disease caused by the gram-negative coccobacillus *F. tularensis* [5, 6]. *F. tularensis* causes the most severe, often fatal, form of the disease through inhalation of as few as ten organisms. However, *F. tularensis* is most transmitted through direct contact with infected animal carcasses such as rodents and rabbits, consumption of contaminated food or water, or through arthropod bites, particularly ticks [7-17]. Due to its extremely low infectious dose and high mortality rate along with its potential use as a biological warfare agent, *F. tularensis* is classified by the Center for Disease Control and Prevention (CDC) as a Category A select agent [5, 18]. People typically become infected after touching or moving diseased or infected dead animals resulting in skin ulcers or respiratory tularemia, consuming or coming in contact with contaminated food or water, and by arthropod vectors to include tick bites [8-10, 13, 22-24]. Tularemia clinical cases have been reported around the world, people who become infected after having been exposed to *F. tularensis* generally develop symptoms of disease within three to five days of exposure [17, 34, 35]. Although symptoms of tularemia depend largely upon the strain and route of infection, ulceroglandular tularemia and glandular tularemia are the most common forms of the disease. These two common clinical manifestations would be known as primary clinical presentations of disease prior to presentation of tularemia meningitis. Identification of tularemia meningitis is a difficult task given it takes no less than one week, and in some cases up to two weeks to get a proper meningitis diagnosis, meanwhile during this time patients are misdiagnosed.

Previous published articles describe tularemia meningitis in a clinical setting with patients' medical history, presenting symptoms, diagnosis, and course of treatment, however, they have

failed to explore this disease further. This study represents a new infection modality for *F. tularensis* and another bacterium that is aggregated to the list of privileged pathogens with the capability of productively infecting brain tissue. Our data show evidence of active infection in brain tissue of intradermally infected mice with LVS.

Our data showed evidence of active infection in brain tissue that began accumulating 42 hours post-infection and peaked at 60 hours post-infection. We detected that microglia, astrocytes, and oligodendrocytes were infected by LVS, however, the largest infected cell population was observed to be peripheral macrophages suggesting to a possible mechanism. When testing this hypothesis, it was found that by depleting macrophages from an infected transgenic mouse model, all LVS signal was lost when compared to controls. This further suggested that peripheral macrophages may be carrying LVS into the brain. To further test this hypothesis, with the use of an *in vitro* BBB model, purified infected macrophages demonstrated a high level of transit across the endothelial blood-brain barrier model thereby corroborating our previous data. Finally, this study has also confirmed an active inflammatory response in the CNS following peripheral inoculation both in general and regional brain tissue with IL-1 β , IL-6, IFN- γ , and TNF- α , all markers that are classically indicative of an inflammatory response.

Further studies are needed to identify other possible cell targets of LVS in the CNS. It cannot be discarded that infected macrophages from the periphery are crossing into the brain in large quantities due to a compromised BBB due to the inflammation levels happening after infection. This would warrant further studies of the BBB after infection with *F. tularensis* to determine if a leaky or otherwise compromised BBB is occurring due to the high inflammation levels seen following infection. Indeed, peripheral macrophages repopulate in the CD11b-DTR mouse model after withdrawal of DT, and further experiments with the use of a complete

macrophage knockout mouse model might be appropriate to address this concern. This study also opens the question for *F. tularensis*' use of alternative mechanisms for traversing the BBB as is the case with *L. monocytogenes* and *M. tuberculosis*. Each of these pathogens use a transmigration or "Trojan Horse" pathway, however, they both also use a paracellular mechanism to cross the BBB. Furthermore, it would be compelling to explore the motive an LVS-infected macrophage would have to transmigrate into the CNS. Indeed, there is a spread of the inflammatory response, it would be necessary to explore the distribution of *F. tularensis* within the brain, and in conjunction study the corresponding spread of inflammation to explore if the resulting inflammation from *F. tularensis* neuroinvasion could lead to damage to neurons and other cells in these regions. Therefore, it is possible that cognitive or behavioral disorders arise following infection and thus should be explored as well. It would also be interesting to explore the translational aspect into human disease, does *F. tularensis* infiltration of the CNS cause damage in human infections as well, if so, how long lasting are these effects?

References

1. Liu, T.B., D. Perlin, and C. Xue, *Molecular mechanisms of cryptococcal meningitis*. *Virulence*, 2012. **3**(2): p. 173-181.
2. Kim, K.S., *How pathogens penetrate the blood-brain barrier*. *Microbe Magazine*, 2014. **9**(12).
3. Kim, K.S., *Mechanisms of microbial traversal of the blood-brain barrier*. *Nature Reviews Microbiology*, 2008. **6**(8): p. 625-34.
4. Kim, K.S., *Microbial translocation of the blood–brain barrier*. *International Journal for Parasitology*, 2006. **36**(5): p. 607-614.
5. Sharma, J., et al., *Features of sepsis caused by pulmonary infection with Francisella tularensis Type A strain*. *Microbial Pathogenesis*, 2011. **51**(1-2): p. 39-47.
6. McCoy, G.W. and C.W. Chapin, *Studies of plague, a plague-like disease, and tuberculosis among rodents in California*. U.S. Public health service. Public health bulletin. 1912, Washington: Government Printing Office. 30 p.
7. Sjostedt, A., *Tularemia: history, epidemiology, pathogen physiology, and clinical manifestations*. *Annals of the New York Academy of Sciences*, 2007. **1105**: p. 1-29.
8. Berdal, B.P., et al., *Field investigations of tularemia in Norway*. *FEMS Immunology and Medical Microbiology*, 1996. **13**: p. 191-195.
9. Berdal, B.P., et al., *Field detection of Francisella tularensis*. *Scandinavian Journal of Infectious Diseases*, 2000. **32**(3): p. 287-291.
10. Mörner, T., *The ecology of tularaemia*. *Revue Scientifique et Technique-Office International des Épizooties*, 1992. **11**: p. 1123-1123.

11. Helvacı, S., et al., *Tularemia in Bursa, Turkey: 205 cases in ten years*. European Journal of Epidemiology, 2000. **16**(3): p. 271-276.
12. Tärnvik, A., G. Sandström, and A. Sjöstedt, *Epidemiological analysis of tularemia in Sweden 1931–1993*. FEMS Immunology and Medical Microbiology, 1996. **13**(3): p. 201-204.
13. Mörner, T. and K. Sandstedt, *A serological survey of antibodies against Francisella tularensis in some Swedish mammals*. Nordisk Veterinærmedicin, 1983. **35**(2): p. 82-85.
14. Mörner, T., et al., *Identification and classification of different isolates of Francisella tularensis*. Journal of Veterinary Medicine, Series B, 1993. **40**(1-10): p. 613-620.
15. Boyce, J.M., *Recent Trends in the Epidemiology of Tularemia in the United States*. Journal of Infectious Diseases, 1975. **131**(2): p. 197-199.
16. Stewart, S.J., *Tularemia: association with hunting and farming*. FEMS Immunology & Medical Microbiology, 1996. **13**(3): p. 197-199.
17. Kilic, S. *A general overview of Francisella tularensis and the epidemiology of tularemia in Turkey*. 2010 June 2019]; Available from: http://www.floradergisi.org/getFileContent.aspx?op=html&ref_id=153&file_name=2010-15-2-037-058.htm&_pk=3fa2a8b6-e964-4606-a36b-b3898d86ea1f.
18. Dennis, D.T., et al., *Tularemia as a biological weapon: medical and public health management*. JAMA, 2001. **285**(21): p. 2763-2773.
19. CDC. *Bioterrorism agents/diseases*. [cited 2019 May 5]; Available from: <https://emergency.cdc.gov/agent/agentlist-category.asp>.
20. CDC. *Basic laboratory protocols for the presumptive identification of Francisella tularensis* 2001 [cited 2019 April 15].

21. Mangold, T. and J. Goldberg, *Plague wars: a true story of biological warfare*. . Vol. First Edition. 2000, United Kingdom: Mcmillan Publishers Ltd. 416.
22. Hermanowska-Szpakowicz, T. and S.A. Pancewicz, *The presence of antibodies against Francisella tularensis among inhabitants of North-Eastern Poland*. Przegląd Epidemiologiczny, 1996. **50**(1-2): p. 55-59.
23. Lévesque, B., et al., *Seroepidemiologic study of three zoonoses (leptospirosis, Q fever, and tularemia) among trappers in Québec, Canada*. Clinical Diagnostic Laboratory Immunology, 1995. **2**(4): p. 496-498.
24. Syrjälä, H., et al., *Airborne transmission of tularemia in farmers*. Scandinavian Journal of Infectious Diseases, 1985. **17**(4): p. 371-375.
25. Olsufjev, N.G., *Taxonomy and characteristic of the genus Francisella dorofeev*. Journal of Hygiene, Epidemiology, Microbiology, and Immunology, 1970. **14**(1): p. 67-74.
26. Staples, J.E. and e. al., *Epidemiologic and molecular analysis of human tularemia, United States, 1964-2004*. Emerging Infectious Diseases, 2006. **12**(7): p. 1113-1118.
27. Harik, N.S., *Tularemia: epidemiology, diagnosis, and treatment*. Pediatric Annals, 2013. **42**(7): p. 288-292.
28. Burke, D.S., *Immunization against tularemia: analysis of the effectiveness of live Francisella tularensis vaccine in prevention of laboratory-acquired tularemia*. Journal of Infectious Diseases, 1977. **135**(1): p. 55-60.
29. McCrumb Jr, F.R., *Aerosol infection of man with Pasteurella tularensis*. Bacteriological Reviews, 1961. **25**(3): p. 262.
30. Saslaw, S., et al., *Tularemia vaccine study: II. Respiratory challenge*. Archives of Internal Medicine, 1961. **107**(5): p. 702-714.

31. Hornick, R.B. and H.T. Eigelsbach, *Aerogenic immunization of man with live Tularemia vaccine*. Bacteriological Reviews, 1966. **30**(3): p. 532.
32. Ellis, J., et al., *Tularemia*. Clinical Microbiology Reviews, 2002. **15**(4): p. 631-46.
33. CDC. *Transmission*. 2018; Available from: <https://www.cdc.gov/tularemia/transmission/index.html>.
34. Evans, M.E., et al., *Tularemia: a 30-year experience with 88 cases*. Medicine, 1985. **64**(4): p. 251-269.
35. Ohara, Y., et al., *Clinical manifestations of tularemia in Japan—analysis of 1,355 cases observed between 1924 and 1987*. Infection, 1991. **19**(1): p. 14-17.
36. Tärnvik, A., et al., *Orchestration of the protective immune response to intracellular bacteria: Francisella tularensis as a model organism*. FEMS Immunology and Medical Microbiology, 1996. **13**(3): p. 221-225.
37. Steinemann, T.L., et al., *Oculoglandular tularemia*. Archives of Ophthalmology, 1999. **117**(1): p. 132-133.
38. Bakış, B. and S. Kılıç. *A General Overview of Francisella tularensis and the Epidemiology of Tularemia in Turkey*. 2011.
39. Marks, L. and A. Spec, *Glandular Tularemia*. New England Journal of Medicine, 2018. **379**(10): p. 967-967.
40. Hajjar, A.M., et al., *Lack of In Vitro and In Vivo Recognition of Francisella tularensis Subspecies Lipopolysaccharide by Toll-Like Receptors*. Infection and Immunity, 2006. **74**(12): p. 6730-6738.
41. Raetz, C.R.H., et al., *Discovery of new biosynthetic pathways: the lipid A story*. Journal of Lipid Research, 2009. **50 Suppl**(Suppl): p. S103-S108.

42. Peng, K., et al., *Elevated AIM2-mediated pyroptosis triggered by hypercytotoxic Francisella mutant strains is attributed to increased intracellular bacteriolysis*. Cellular Microbiology, 2011. **13**(10): p. 1586-600.
43. Henry, T., et al., *Type I interferon signaling is required for activation of the inflammasome during Francisella infection*. Journal of Experimental Medicine, 2007. **204**(5): p. 987-94.
44. Celli, J. and T.C. Zahrt, *Mechanisms of Francisella tularensis intracellular pathogenesis*. Cold Spring Harbor Perspectives in Medicine, 2013. **3**(4): p. a010314.
45. Kinkead, L.C. and L.A. Allen, *Multifaceted effects of Francisella tularensis on human neutrophil function and lifespan*. Immunological Reviews 2016. **273**(1): p. 266-81.
46. Clemens, D.L., B.Y. Lee, and M.A. Horwitz, *Virulent and avirulent strains of Francisella tularensis prevent acidification and maturation of their phagosomes and escape into the cytoplasm in human macrophages*. Infection and Immunity, 2004. **72**(6): p. 3204-17.
47. Wehrly, T.D., et al., *Intracellular biology and virulence determinants of Francisella tularensis revealed by transcriptional profiling inside macrophages*. Cellular Microbiology, 2009. **11**(7): p. 1128-50.
48. Jones, J.W., P. Broz, and D.M. Monack, *Innate immune recognition of Francisella tularensis: activation of type-I interferons and the inflammasome*. Frontiers in Microbiology, 2011. **2**: p. 16-16.
49. Mares, C.A., et al., *Defect in efferocytosis leads to alternative activation of macrophages in Francisella infections*. Immunology and Cell Biology, 2011. **89**(2): p. 167-72.
50. Sharma, J., et al., *TLR4-dependent activation of inflammatory cytokine response in macrophages by Francisella elongation factor Tu*. Cellular Immunology, 2011. **269**(2): p. 69-73.

51. Tyler, K.L., *Chapter 28: a history of bacterial meningitis*. Handbook Clinical Neurology, 2010. **95**: p. 417-33.
52. Hull, C.M. and J. Heitman, *Genetics of Cryptococcus neoformans*. Annual Review of Genetics, 2002. **36**: p. 557-615.
53. Wu, Y., et al., *Microglia and amyloid precursor protein coordinate control of transient Candida cerebritis with memory deficits*. Nature Communications, 2019. **10**(1): p. 58.
54. Zou, H., et al., *Cerebral hemorrhage due to tuberculosis meningitis: a rare case report and literature review*. Oncotarget, 2015. **6**(42): p. 45005-45009.
55. Uysal, G., et al., *Magnetic resonance imaging in diagnosis of childhood central nervous system tuberculosis*. Infection, 2001. **29**(3): p. 148-153.
56. van Samkar, A., et al., *Zoonotic bacterial meningitis in human adults*. Neurology, 2016. **87**(11): p. 1171-9.
57. Hickman, H.D. and T.C. Pierson, *Zika in the Brain: New Models Shed Light on Viral Infection*. Trends in Molecular Medicine, 2016. **22**(8): p. 639-641.
58. Byrne, S.N., et al., *Interleukin-1 β but not tumor necrosis factor is involved in West Nile virus-induced Langerhans cell migration from the skin in C57BL/6 mice*. Journal of Investigative Dermatology, 2001. **117**(3): p. 702-709.
59. Lim, P.Y., et al., *Keratinocytes are cell targets of West Nile virus in vivo*. Journal of Virology, 2011. **85**(10): p. 5197-5201.
60. Welte, T., et al., *Toll-like receptor 7-induced immune response to cutaneous West Nile virus infection*. The Journal of General Virology, 2009. **90**(Pt 11): p. 2660.

61. Pron, B., et al., *Interaction of Neisseria meningitidis with the Components of the Blood-Brain Barrier Correlates with an Increased Expression of PilC*. The Journal of Infectious Diseases, 1997. **176**(5): p. 1285-1292.
62. Nassif, X., et al., *How do extracellular pathogens cross the blood-brain barrier?* Trends in Microbiology, 2002. **10**(5).
63. Hofinger, D.M., et al., *Tularemic meningitis in the United States*. JAMA, 2009. **66**(4): p. 523-527.
64. Owens, I.P., *Ecology and evolution. Sex differences in mortality rate*. Science, 2002. **297**(5589): p. 2008-9.
65. Giefing-Kröll, C., et al., *How sex and age affect immune responses, susceptibility to infections, and response to vaccination*. Aging Cell, 2015. **14**(3): p. 309-321.
66. van Lunzen, J. and M. Altfeld, *Sex differences in infectious diseases—common but neglected*. The Journal of Infectious Diseases, 2014. **209**(suppl_3): p. S79-S80.
67. Sunagar, R., et al., *Vaccination evokes gender-dependent protection against tularemia infection in C57BL/6Tac mice*. Vaccine, 2016. **34**(29): p. 3396-3404.
68. Louveau, A., et al., *CNS lymphatic drainage and neuroinflammation are regulated by meningeal lymphatic vasculature*. Nature Neuroscience, 2018. **21**(10): p. 1380-1391.
69. Skaper, S.D., et al., *Neuroinflammation, Mast Cells, and Glia: Dangerous Liaisons*. Neuroscientist, 2017. **23**(5): p. 478-498.
70. Duarte-Delgado, N.P., G. Vásquez, and B.L. Ortiz-Reyes, *Blood-brain barrier disruption and neuroinflammation as pathophysiological mechanisms of the diffuse manifestations of neuropsychiatric systemic lupus erythematosus*. Autoimmunity Reviews, 2019. **18**(4): p. 426-432.

71. Benveniste, E.N., et al., *Induction and regulation of interleukin-6 gene expression in rat astrocytes*. Journal of Neuroimmunology, 1990. **30**(2-3): p. 201-212.
72. Aloisi, F., et al., *Production of hemolymphopoietic cytokines (IL-6, IL-8, colony-stimulating factors) by normal human astrocytes in response to IL-1 beta and tumor necrosis factor-alpha*. The Journal of Immunology, 1992. **149**(7): p. 2358-2366.
73. Ringheim, G.E., K.L. Burgher, and J.A. Heroux, *Interleukin-6 mRNA expression by cortical neurons in culture: evidence for neuronal sources of interleukin-6 production in the brain*. Journal of Neuroimmunology, 1995. **63**(2): p. 113-123.
74. Erta, M., A. Quintana, and J. Hidalgo, *Interleukin-6, a major cytokine in the central nervous system*. International Journal of Biological Sciences, 2012. **8**(9): p. 1254-1266.
75. Shaftel, S.S., W.S.T. Griffin, and M.K. O'Banion, *The role of interleukin-1 in neuroinflammation and Alzheimer disease: an evolving perspective*. Journal of Neuroinflammation, 2008. **5**(1): p. 7.
76. Sun, L., et al., *Neuroprotection by IFN- γ via astrocyte-secreted IL-6 in acute neuroinflammation*. Oncotarget, 2017. **8**(25): p. 40065-40078.
77. Montgomery, S.L. and W.J. Bowers, *Tumor necrosis factor-alpha and the roles it plays in homeostatic and degenerative processes within the central nervous system*. Journal of Neuroimmune Pharmacology, 2012. **7**(1): p. 42-59.
78. Clark, I.A., *How TNF was recognized as a key mechanism of disease*. Cytokine and Growth Factor Reviews, 2007. **18**(3-4): p. 335-343.
79. Santello, M. and A. Volterra, *TNF α in synaptic function: switching gears*. Trends in Neurosciences, 2012. **35**(10): p. 638-647.

80. Beattie, E.C., et al., *Control of synaptic strength by glial TNF α* . Science, 2002. **295**(5563): p. 2282-2285.
81. Kaneko, M., et al., *Tumor necrosis factor- α mediates one component of competitive, experience-dependent plasticity in developing visual cortex*. Neuron, 2008. **58**(5): p. 673-680.
82. Baune, B.T., et al., *Cognitive dysfunction in mice deficient for TNF-and its receptors*. American Journal of Medical Genetics Part B: Neuropsychiatric Genetics, 2008. **147**(7): p. 1056-1064.
83. Beste, C., et al., *Variations in the TNF- α gene (TNF- α -308G \rightarrow A) affect attention and action selection mechanisms in a dissociated fashion*. Journal of Neurophysiology, 2010. **104**(5): p. 2523-2531.
84. Krueger, J.M., *The role of cytokines in sleep regulation*. Current Pharmaceutical Design, 2008. **14**(32): p. 3408-3416.
85. McCoy, M.K. and M.G. Tansey, *TNF signaling inhibition in the CNS: implications for normal brain function and neurodegenerative disease*. Journal of Neuroinflammation, 2008. **5**(1): p. 45.
86. Council, N.R., *Guide for the Care and Use of Laboratory Animals: Eighth Edition*. 2011, Washington, DC: The National Academies Press. 246.
87. Ghosh, P., et al., *Invasion of the Brain by *Listeria monocytogenes* Is Mediated by *InlF* and Host Cell Vimentin*. mBio, 2018. **9**(1): p. e00160-18.
88. Iovino, F., et al., *Interactions between Blood-Borne Streptococcus pneumoniae and the Blood-Brain Barrier Preceding Meningitis*. PLOS ONE, 2013. **8**(7): p. e68408.

89. Rock, R.B., et al., *Mycobacterium tuberculosis*–Induced Cytokine and Chemokine Expression by Human Microglia and Astrocytes: Effects of Dexamethasone. *The Journal of Infectious Diseases*, 2005. **192**(12): p. 2054-2058.
90. Le Monnier, A., et al., *ActA is required for crossing of the fetoplacental barrier by Listeria monocytogenes*. *Infect Immun*, 2007. **75**(2): p. 950-7.
91. Iovino, F., et al., *How Does *Streptococcus pneumoniae* Invade the Brain?* *Trends in Microbiology*, 2016. **24**(4): p. 307-315.
92. Lee, S.C., et al., *Cytokine production by human fetal microglia and astrocytes. Differential induction by lipopolysaccharide and IL-1 beta*. *J Immunol*, 1993. **150**(7): p. 2659-67.
93. Hashioka, S., et al., *Antidepressants inhibit interferon-gamma-induced microglial production of IL-6 and nitric oxide*. *Exp Neurol*, 2007. **206**(1): p. 33-42.
94. Benveniste, E.N., et al., *Induction and regulation of interleukin-6 gene expression in rat astrocytes*. *J Neuroimmunol*, 1990. **30**(2-3): p. 201-12.
95. Sawada, M., A. Suzumura, and T. Marunouchi, *TNF alpha induces IL-6 production by astrocytes but not by microglia*. *Brain Res*, 1992. **583**(1-2): p. 296-9.
96. Borison, H.L. and K.R. Brizzee, *Morphology of emetic chemoreceptor trigger zone in cat medulla oblongata*. *Proc Soc Exp Biol Med*, 1951. **77**(1): p. 38-42.
97. Curtis, K.S., et al., *Impaired osmoregulatory responses in rats with area postrema lesions*. *Am J Physiol*, 1999. **277**(1): p. R209-19.
98. Johnstone, L.E., T.M. Fong, and G. Leng, *Neuronal activation in the hypothalamus and brainstem during feeding in rats*. *Cell Metab*, 2006. **4**(4): p. 313-21.
99. Smith, P.M., et al., *Leptin influences the excitability of area postrema neurons*. *Am J Physiol Regul Integr Comp Physiol*, 2016. **310**(5): p. R440-8.

100. Goehler, L.E., A. Erisir, and R.P. Gaykema, *Neural-immune interface in the rat area postrema*. Neuroscience, 2006. **140**(4): p. 1415-34.
101. Langlet, F., et al., *Tanycyte-like cells form a blood-cerebrospinal fluid barrier in the circumventricular organs of the mouse brain*. J Comp Neurol, 2013. **521**(15): p. 3389-405.
102. Willis, C.L., C.J. Garwood, and D.E. Ray, *A size selective vascular barrier in the rat area postrema formed by perivascular macrophages and the extracellular matrix*. Neuroscience, 2007. **150**(2): p. 498-509.
103. Al-Saleh, S.S., C. Kaur, and E.A. Ling, *Response of neurons and microglia/macrophages in the area postrema of adult rats following exposure to hypobaric hypoxia*. Neuroscience Letters, 2003. **346**(1): p. 77-80.
104. Brizzee, K.R. and P.M. Klara, *The structure of the mammalian area postrema*. Fed Proc, 1984. **43**(15): p. 2944-8.
105. Nakano, Y., et al., *Astrocytic TLR4 expression and LPS-induced nuclear translocation of STAT3 in the sensory circumventricular organs of adult mouse brain*. J Neuroimmunol, 2015. **278**: p. 144-58.
106. Tsai, S.-J., *Effects of interleukin-1beta polymorphisms on brain function and behavior in healthy and psychiatric disease conditions*. Cytokine & Growth Factor Reviews, 2017. **37**: p. 89-97.

Vita

Mireya Griselle Ramos-Muniz was born on August 9, 1988 in Ciudad Juarez, Chihuahua, Mexico. She graduated Coronado High School, then enrolled at El Paso Community College followed by enrollment at The University of Texas at El Paso where she earned a Bachelor of Science in Biology degree. In the Fall of 2014, she enrolled in the Master of Science in Biology program at UTEP, then applied and was accepted into the doctoral program the in the Fall of 2015.

During her time in the graduate program, she was awarded an Outstanding Masters Student in the Pathobiology Program award by the Department of Biological Sciences at UTEP in 2015. She was also awarded the National Institute of General Medical Sciences (NIGMS) Ancillary Training Program Scholarship, a travel scholarship to the Keystone Symposium on Neuroinflammation in Diseases of the Central Nervous System. She has mentored numerous students in the lab during her graduate studies, and served as a Teaching Assistant for multiple upper division lab courses. She has presented her research at multiple national meetings for the American Association of Immunologists, the Society for Neuroscience, and Keystone Symposium. She may be contacted at mireyagramos@gmail.com.